

Supplementary Information

Contents

Appendix S1. Site Details	2
Appendix S2. Methods for reconstruction of <i>DBH</i>	3
Appendix S3. Methods for climate data evaluation and correction	4
Appendix S4. Methods for comparing our approach with traditional methods	5
Appendix S5. Dealing with rapidly changing climate and tree growth	7
Appendix S6. Analysis of DBH-growth relationships by decade	8
Table S1. Site Details.	9
Table S2. Species analyzed, their characteristics, and bark allometries applied.	10
Table S3. Sampling details for species by site.	11
Table S4. Allometric equations for bark thickness.	13
Table S5. Qualitative comparison of results from this study with previous studies employing conventional methods.	14
Figure S1. Comparison of our approach with traditional methods of identifying climate signals: LITU at SCBI.	17
Figure S2. Comparison of our approach with traditional methods of identifying climate signals: ABAL at Zofin.	18
Figure S3. Comparison of our approach with traditional methods of identifying climate signals: PSME at Cedar Breaks.	19
Figure S4. Comparison of our approach with traditional methods of identifying climate signals: PIMA at Scotty Creek.	20
Figure S5. (PRE at SCBI)	21
Figure S6. (PET at SCBI)	22
Figure S7. (TMX/TMP at HKK)	23
Figure S9. Best GLS models for Barro Colorado Island (Panama)	24
Figure S10. Best GLS models for Huai Kha Khaeng (Thailand)	25
Figure S11. Best GLS models for the Smithsonian Conservation Biology Institute (Virginia, USA)	26
Figure S12. Best GLS models for Lilley Dickey Woods (Indiana, USA)	27
Figure S13. Best GLS models for Harvard Forest (Massachusetts, USA)	28
Figure S14. Best GLS models for Zofin Forest (Czech Republic)	29
Figure S15. Best GLS models for Niobrara/ Halsey (Nebraska, USA)	30
Figure S16. Best GLS models for Little Tesuque (New Mexico, USA)	31
Figure S17. Best GLS models for Cedar Breaks (Utah, USA)	32
Figure S18. Best GLS models for Scotty Creek (Northwest Territory, Canada)	33
SI References	34

Appendix S1. Site Details

(include descriptions of stand history, global change dynamics)

Barro Colorado Island, Panama

Huai Kha Khaeng, Thailand

Smithsonian Conservation Biology Institute, Virginia, USA

Lilly Dickey Woods, Indiana, USA

Harvard Forest, USA

Žofín Forest Dynamics Plot, Czech Republic

Niobrara, Nebraska, USA

Riparian site BEPA are growing on N facing slopes near stream

Little Tesuque, New Mexico, USA

Cedar Breaks, Utah, USA

Scotty Creek, Northwest Territories, Canada

melting permafrost

Appendix S2. Methods for reconstruction of DBH

This is still rough/ mostly notes.

In most cases, when a recent *DBH* measurement was available, *DBH* was reconstructed from the outside in. In cases where *DBH* was not available, but when we knew that the core hit pith or could reasonably estimate how far off it was based on the curvature of the rings (Applequist, 1958; Duncan, 1989), *DBH* was reconstructed from the inside out.

For each core, *DBH* can be reconstructed outside-in (based on recent *DBH*, subtracting growth recorded in tree rings) or inside-out (summing *RW* from the inside out,—only when core hit pith or distance to pith can be reliably estimated). We generally gave precedence to the outside-in approach. Specifically, when *DBH* was taken at the time of coring,

At some of our sites where *DBH* was not taken at the time of coring (*SCBI*), *DBH* measurements taken before or slightly after the time of coring could be used. (see issue #19 in *ForestGEO_dendro*) If before, ... If after... For all outside-in reconstructions, if a negative *DBH* was predicted...

When there were more than one cores for a tree, the *DBH* reconstructions from each core were averaged to produce a single estimate of the tree's *DBH* through time. When the start or end dates of the records from the cores differed, we extrapolated growth of the shorter core to match the years covered by the longer core. Specifically, to fill in years at the more recent end, we assumed that the average growth rate of the ten years prior to the missing records applied to the missing years. To fill in years at the beginning of the tree's lifespan, we likewise assumed that the ten years adjacent to the missing record applied to the missing years; however, if this yielded a negative *DBH* estimate for the earliest year in the reconstruction, we divided the existing minimum *DBH* by number of years missing and applied that value to each year. We note that these reconstructed growth records were used only for the reconstruction of *DBH* and were not included as response variables in any of our analyses.

In either case we need bark thickness—ideally allometries describing the relationship between *DBH* and bark thickness (Table S4). This is especially critical for thick-barked species. When bark thickness data were available, we generated allometries (issue #8 in *ForestGEO_dendro*)... lognormal model with intercept forced to zero: `lm(bark_depth.mm ~ -1 + log(dbh_no_bark.cm+1):bark_species, data = bark)`. When bark thickness data were not available, we used published bark allometries from other sources (Table S4)

Appendix S3. Methods for climate data evaluation and correction

For BCI, we calculated monthly PPT and PDF from daily precipitation readings made on BCI starting in 1929 (Paton, 2019).

Appendix S4. Methods for comparing our approach with traditional methods

To test whether our methods gave similar results to traditional methods, we conducted qualitative comparisons of our results to previous studies based on the same cores (Table S5) and conducted a formal quantitative comparison for four species (Figs. S1-S4), as detailed below.

Qualitative comparison

For all species-site combinations, we reviewed previous studies characterizing the climate sensitivity of growth using conventional methods. In most cases, we were able to compare with previous studies from the same sites and sets of cores. When these were not available, we reviewed regional-level analyses believed to be representative of the site.

Results from previous studies were compiled alongside results from the climate-only model in this study (Table S5). Where previous studies examined numerous climate variables or time windows (e.g., Helcoski et al., 2019), we focus on those most relevant to our findings.

Beyond the methodological differences, original studies based on the same sets of cores varied from this one and from one another in factors including the exact set of cores analyzed, climate data sources, time frame of analysis, approaches to identifying candidate climate variables and windows (including whether this is done on a site or species level), methods for detrending and standardizing to build chronologies, and whether the effects of temperature and precipitation are considered separately (original studies) or additively (this study). To standardize for such differences, we selected a subset of species for a standardized quantitative comparison, as detailed below.

Quantitative comparison

We also conducted a formal comparison of our approach to conventional methods using identical tree-ring and climate data for four species: PSME (Cedar Breaks, Utah), ABAL (*Žofín*), PIMA (Scotty Creek), and LITU (SCBI; Figs. S1-S4). These species were selected for analysis because they have been well-studied in the past. For each species, we compared climate sensitivities for the top precipitation- and temperature-group variables, as identified in the main analysis.

Prior to analysis, data were prepared and cleaned as described in the Methods section, resulting in an identical set of records for input into each analysis. For the approach developed here, analysis was conducted as described in the Methods section, but with the *climwin* climate variable selection process limited to just the species of interest (as opposed to all species at the site), climate variables considered individually rather than additively, analysis of only first-order linear relationships, and with start date adjusted to match the conventional method (see below). Following the *climwin* analysis step, we extracted *beta* coefficients describing the slope of the relationship between climate and *RW*. *Beta* coefficients, along with their standard error, were obtained for each month within the analysis time frame (Table S1) and for the time window identified as optimal by *climwin*.

For the analysis using conventional methods, the ring-width series from each core was standardized via ARSTAN using a 2/3rds n spline, where n is the number of years in the series (Cook, 1985; Cook & Kairiukstis, 1990). (*The following italic text is self-plagiarized from Helcoski and needs to be reworded:*) *The influence of outliers in all series was reduced using the adaptive power transformation, which also stabilises the variance over time (Cook & Peters, 1997). Next, each series was stabilised using either the average correlation between raw ring-width series (*rbar*) method or a 1/3rds spline method to adjust changes in variance as series replication decreased towards the earlier portion of each chronology (Jones et al., 1997). The 1/3rds spline method was chosen when replication in the inner portion of each chronology (c. the inner 30–50 yr of each record depending on full chronology length) dropped below three trees. Once that step was complete, a robust biweight mean chronology for each species was calculated from the ring-width indices (Cook, 1985). We chose to use residual chronologies because the autoregressive standardisation process in creating them removes much of the tree-level autocorrelation in growth and these chronologies would most likely contain the most conservative information on drivers of interannual growth (Cook, 1985).*

We defined chronology start dates according to the subsample signal strength (SSS), using a cutoff of SSS = 0.80 (or 80% of the population signal). Thus, for this analysis only, we defined chronology start dates as the

year the SSS exceeded 0.80 or two years after the start of the climate record, whichever came later. SSS exceeded 0.80 well before the start of the 1901 start of climate records for PSME (1800s), ABAL (1700), and PIMA (1850s). For LITU, SSS reached 0.8 with 11 trees in 1919, which we used as the start date for this series. We note that these start date criteria differ from those used in the main analysis (Table S3), which had earlier start dates because the analysis was not constrained by a need to represent the full population signal. End dates were defined as the last full year prior to sampling (Table S3).

Beta (slope) coefficients for the relationship between tree growth and the monthly climate variable were derived as in Helcoski et al. (2019): (*SELF-PLAGIARIZED CONTENT:*) *Analyses of climate-growth relationships were conducted using ‘dplR’ (Bunn, 2008) and ‘bootRes’ (Zang & Biondi, 2013), which correlated functions and bootstrapped confidence intervals for the relationships between annual growth and monthly climate variables following Biondi & Waikul (2004).* Pearson correlations between climate variables and tree-ring chronologies were converted to linear slopes using the method of Charney et al. (2016).

Finally, we generated plots comparing month-by-month *beta* coefficients describing climate sensitivity, and also comparing *beta* coefficients for the window identified as optimal by *climwin* Figs. S1-S4).

We note that despite designing the analyses to be as comparable as possible, one-to-one correspondence of *beta* coefficients is not necessarily expected for several reasons. First, although the analysis time frame is standardized between the two approaches, the relative influence of each year will generally vary between the two approaches. The traditional approach, which all cores into a single residual chronology with one value per year, gives equal weighting to each year. In contrast, under the approach developed here, the number records per year will vary across the analysis time frame, generally increasing over time as the younger trees enter the analysis. Thus, where many younger trees are included in the analysis, the two approaches will effectively give different weights to the years included in the analysis period. In cases where climate-sensitivity differs between old and young trees, or where the climate and/or climate response changed substantially over the analysis time frame (e.g., at Scotty Creek; Fig. S4; Sniderhan & Baltzer, 2016), this may lead to divergence of the climate sensitivities estimated by the two methods.

Second, traditional analysis methods (using ARSTAN) were primarily designed to distill population-level variation to obtain the strongest possible climate signal for the reconstruction of past climate (**Cook & Kariustis**), not to characterize climate responses on the individual level, where variation is inherently higher. While conversion of Pearson correlations to linear slopes *sensu* Charney et al. (2016) approximates climate responses, it does not provide an exact slope describing the relationship between individual-level or population mean growth and climate. This is because standardization of variance and averaging of individual-level residuals prior to the climate analysis fundamentally alters and obfuscates individual-level responses.

We suspect that both of these factors may underlie the tendency for the traditional method to estimate stronger climate sensitivity than the approach developed here for Scotty Creek (Fig. S4), a comprehensively sampled black spruce forest (i.e., including young trees) on melting permafrost. We note, however, that there are no statistically significant differences in the *beta* coefficients of the two approaches at this site.

Appendix S5. Dealing with rapidly changing climate and tree growth

ISSUE #25 in ForestGEO-climate-sensitivity

Our analysis included two sites where climate change has had pronounced effects on tree growth: Scotty Creek, NW Territories, Canada (SC) and Little Tesuque, New Mexico, USA (LT). At SC, rapidly rising temperatures are causing melting permafrost, summer moisture stress, resulting in negative growth trends in basal area index (*BAI*) starting around 1950 and significant growth declines since 1970 in 56% of trees (Sniderhan & Baltzer, 2016). At LT, increasingly warm drought has dramatically reduced growth (Williams et al., 2012), resulting in many missing rings in recent years.

Problematically, correlating tree growth residuals from which climate-driven trends had been removed against the climate signal with a strong directional trend would not necessarily identify the most relevant climate drivers.

For these sites, we experimented with three approaches to identifying the most important climate drivers (1) the method described above, (2) detrending the climate variables (**AT:prewhitening?**) prior to the climwin step, and (3) splitting analyses into decades before and after 1970 (*sensu* Sniderhan & Baltzer, 2016) (Appendix S5).

**Appendix S6. Analysis of DBH-growth relationships by decade
(CAMERON'S WORK IN THIS REPO)**

Table S1. Site Details.

site code	site name	latitude	longitude	elevation (m.a.s.l.)	cores within ForestGEO plot?	canopy positions	tree statuses	date range	dormant season*	months in climwin
BCI	Barro Colorado Island	9.15430	-79.8461	120-160	no	canopy	live, dead	1931-2014	Nov-Apr	pOct-cDec
HKK	Huai Kha Khaeng	15.63240	99.2170	549-638	no	all	live	1903-2011	Nov-Apr	pOct-cDec
SCBI	Smithsonian Conservation Biology Institute	38.89350	-78.1454	273-338	yes	all	live, dead	1903-2017	Oct-Apr	pMay-cAug
LDW	Lilly Dickey Woods	39.23590	-86.2181	230-303		canopy	live, dead	1903-2019		pMay-cAug
HF	Harvard Forest	42.53880	-72.1755	340-368	yes	all	live, dead	1903-2014		pMay-cAug
ZOF	Zofin Forest Dynamics Plot	48.66380	14.7073	736-829	some	all	live, dead	1903-2013	Oct-Mar	pMay-cAug
NE	Niobrara/Halsey	42.78000	-100.0210	644-702	some	canopy	live		Oct-Apr	pMay-cAug
LT	Little Tesuque	35.73838	-105.8382	2684 - 2702	n.a.	canopy / sub-canopy	live	1903-2018	Oct-Apr	pMay-cAug
CB	Utah Forest Dynamics Plot	37.66150	-112.8525	3020-3169	yes		live	1903-2007		pMay-cAug
SC	Scotty Creek	61.30000	-121.3000	280	no	all	live, dead	1903-2013	Sept-Apr	pMay-cAug

- Refers to approximate period during which woody growth ceases (dry season in the tropics, winter for temperate and boreal sites).

Table S2. Species analyzed, their characteristics, and bark allometries applied.

species code	family	latin name	sites sampled	leaf type	leaf phenology	light requirements*	bark allometry**
ABAL	Pinaceae	<i>Abies alba</i>	ZOF	needleleaf	evergreen	shade-tolerant	<i>Abies lasiocarpa</i>
ABBI	Pinaceae	<i>Abies bifolia</i>	CB	needleleaf	evergreen		<i>Abies lasiocarpa</i>
ACRU	Sapindaceae	<i>Acer rubrum</i>	HF	broadleaf	deciduous (cold)		<i>Acer rubrum</i>
ACSA	Sapindaceae	<i>Acer saccharum</i>	LDW	broadleaf	deciduous (cold)		<i>Acer rubrum</i>
AFXY	Fabaceae	<i>Afzelia xylocarpa</i>	HKK	broadleaf	deciduous (drought)		<i>neglected</i>
BEAL	Betulaceae	<i>Betula alleghaniensis</i>	HF	broadleaf	deciduous (cold)		<i>Betula alleghaniensis</i>
BEPA	Betulaceae	<i>Betula papyrifera</i>	Niobara	broadleaf	deciduous (cold)		<i>Betula papyrifera</i>
CACO	Juglandaceae	<i>Carya cordiformis</i>	SCBI	broadleaf	deciduous (cold)		<i>Carya cordiformis</i>
CAGL	Juglandaceae	<i>Carya glabra</i>	SCBI	broadleaf	deciduous (cold)		<i>Carya glabra</i>
CAOV	Juglandaceae	<i>Carya ovata</i>	LDW	broadleaf	deciduous (cold)		<i>Carya glabra</i>
CAOVL	Juglandaceae	<i>Carya ovalis</i>	SCBI	broadleaf	deciduous (cold)		<i>Carya ovalis</i>
CATO	Juglandaceae	<i>Carya tomentosa</i>	SCBI	broadleaf	deciduous (cold)		<i>Carya tomentosa</i>
CHTA	Meliaceae	<i>Chukrasia tabularis</i>	HKK	broadleaf	brevi-deciduous (drought)		<i>neglected</i>
FAGR	Fagaceae	<i>Fagus grandifolia</i>	HF, SCBI	broadleaf	deciduous (cold)		<i>neglected</i>
FASY	Fagaceae	<i>Fagus sylvatica</i>	ZOF	broadleaf	deciduous (cold)	shade-tolerant	<i>neglected</i>
FRAM	Oleaceae	<i>Fraxinus americana</i>	LDW, SCBI	broadleaf	deciduous (cold)		<i>Fraxinus americana</i>
FRNI	Oleaceae	<i>Fraxinus nigra</i>	SCBI	broadleaf	deciduous (cold)		<i>Fraxinus americana</i>
JACO	Bignoniaceae	<i>Jacaranada copaia</i>	BCI	broadleaf	deciduous (drought)	light-demanding	<i>Jacaranada copaia</i>
JUNI	Juglandaceae	<i>Juglans nigra</i>	SCBI	broadleaf	deciduous (cold)		<i>Juglans nigra</i>
JUVI	Cupressaceae	<i>Juniperus virginiana</i>	Hansley	needleleaf	evergreen		<i>neglected</i>
LITU	Magnoliaceae	<i>Liriodendron tulipifera</i>	LDW, SCBI	broadleaf	deciduous (cold)		<i>Liriodendron tulipifera</i>
MEAZ	Meliaceae	<i>Melia azedarach</i>	HKK	broadleaf	deciduous (drought)	light-demanding	<i>neglected</i>
PIAB	Pinaceae	<i>Picea abies</i>	HF	needleleaf	evergreen	intermediate	<i>Picea engelmannii</i>
PIEN	Pinaceae	<i>Picea engelmannii</i>	CB	needleleaf	evergreen		<i>Picea engelmannii</i>
PIFL	Pinaceae	<i>Pinus flexilis</i>	CB	needleleaf	evergreen		<i>Pinus monticola</i>
PILO	Pinaceae	<i>Pinus longaeva</i>	CB	needleleaf	evergreen		<i>neglected</i>
PIMA	Pinaceae	<i>Picea mariana</i>	SC	needleleaf	evergreen		<i>Picea mariana</i>
PIPO	Pinaceae	<i>Pinus ponderosa</i>	Hansley, LT	needleleaf	evergreen		<i>Pinus jeffreyi</i>
PIPU	Pinaceae	<i>Pinus pungens</i>	CB	needleleaf	evergreen		<i>Picea engelmannii</i>
PIST	Pinaceae	<i>Pinus strobus</i>	HF, SCBI	needleleaf	evergreen		<i>Pinus strobus</i>
PIST3	Pinaceae	<i>Pinus strobusiformis</i>	LT	needleleaf	evergreen		<i>Pinus monticola</i>
POTR	Salicaceae	<i>Populus tremuloides</i>	CB	broadleaf	deciduous (cold)		<i>Populus tremuloides</i>
PSME	Pinaceae	<i>Pseudotsuga menziesii</i>	CB	needleleaf	evergreen		<i>Pseudotsuga menziesii</i>
QUAL	Fagaceae	<i>Quercus alba</i>	LDW, SCBI	broadleaf	deciduous (cold)		<i>Quercus alba</i>
QUMO	Fagaceae	<i>Quercus montana</i>	LDW, SCBI	broadleaf	deciduous (cold)		<i>Quercus montana</i>
QURU	Fagaceae	<i>Quercus rubra</i>	HF, LDW, SCBI	broadleaf	deciduous (cold)		<i>Quercus rubra</i>
QUVE	Fagaceae	<i>Quercus velutina</i>	LDW, SCBI	broadleaf	deciduous (cold)		<i>Quercus velutina</i>
TEPA	Burseraceae	<i>Tetragastris panamensis</i>	BCI	broadleaf	evergreen	shade-tolerant	<i>Tetragastris panamensis</i>
TOCI	Meliaceae	<i>Toona ciliata</i>	HKK	broadleaf	deciduous (drought)		<i>neglected</i>
TRTU	Meliaceae	<i>Trichilia tuberculata</i>	BCI	broadleaf	evergreen	shade-tolerant	<i>Trichilia tuberculata</i>
TSCA	Pinaceae	<i>Tsuga canadensis</i>	HF	needleleaf	evergreen		<i>Tsuga canadensis</i>

*For extratropical species, light requirements are classified based on the database of Niinemets & Valladares (2006). For tropical species, categorization is based on Alfaro-Sánchez et al. (2017) for BCI and Vlam et al. (2014) for HKK.

**Bark allometry field indicates the species and site sampled to construct the bark allometry. When neither raw data nor an allometric equation for the study species was available, we selected the most appropriate equation that could be located for similar species. Equations are given in Table S4.

Table S3. Sampling details for species by site.

site	species code	all		with DBH		DBH range		date range
		n trees	n cores	n trees	n cores	sampled	reconstructed*	
BCI	JACO	12	18	11	17	30.2-63.5	2.6-56.4	1931-2014
BCI	TEPA	18	29	17	26	22.1-59.5	2.7-49.4	1931-2014
BCI	TRTU	23	37	20	31	20.7-43.6	4.8-41.5	1931-2014
CB	ABBI	22	41	20	37	13.9-54.2	0.6-45.3	1903-2000
CB	PIEN	12	21	10	16	14-54.9	3.6-39.4	1903-2000
CB	PIFL	12	19	11	18	17.6-63.5	4.5-55.4	1903-1998
CB	PILO	17	24	0	0	NA	NA	1903-1999
CB	PIPU	15	28	15	28	22.4-50.8	8.6-48.5	1903-2000
CB	POTR	17	27	17	27	23.6-47.6	7.7-42.4	1903-2000
CB	PSME	10	19	10	19	20.7-64.2	2.6-49.4	1903-1999
Hansley	JUVI	29	60	29	60	16.6-21.5	1.8-18.4	1948-1994
Hansley	PIPO	59	113	57	109	19.3-63	2.9-46.9	1948-1994
HF	ACRU	18	59	18	59	10.1-22.1	0.9-20.4	1903-2013
HF	BEAL	13	44	13	44	10.2-37.9	1.6-20.5	1904-2013
HF	QURU	74	180	73	177	19.5-53	1.1-48.3	1903-2014
HF	TSCA	32	83	32	82	10.6-37	0.6-33.5	1923-2014
HKK	AFXY	39	127	39	127	20.1-98.7	0.1-81.4	1903-2011
HKK	CHTA	28	70	28	70	16-64.6	0.2-59.5	1904-2010
HKK	MEAZ	46	130	46	130	25.6-98.1	3.8-80.3	1914-2011
HKK	TOCI	45	143	45	143	16.6-116.4	1.7-80.5	1903-2011
LDW	ACSA	35	66	34	64	9-64.6	0-52.4	1903-2019
LDW	CAOV	9	18	8	15	unknown	1.4-37.4	1903-2013
LDW	LITU	15	28	14	25	unknown	1.2-69.4	1903-2019
LDW	QUAL	10	20	0	0	NA	NA	1903-2013
LDW	QUMO	10	20	8	16	unknown	1.1-52.4	1903-2013
LDW	QUVE	9	18	0	0	NA	NA	1903-2013
LT	PIPO	10	20	10	20	23.2-52.8	14.6-48.4	1903-2018
LT	PIST3	7	14	7	13	25.7-39.8	4.2-34.4	1903-2018
Niobara	BEPA	28	84	28	84	unknown	0.4-30.5	1948-1995
SCBI	CACO	15	15	14	14	10.62-38.52	1.7-32.2	1903-2015
SCBI	CAGL	39	39	36	36	10.28-52.31	1.6-49.3	1903-2015
SCBI	CAOVL	25	25	24	24	15.11-60.32	2.6-47.2	1903-2015
SCBI	CATO	15	15	14	14	12.86-35.95	3.7-28.4	1903-2015
SCBI	FAGR	76	76	74	74	10.05-41.02	0.1-41.2	1920-2009
SCBI	FRAM	66	66	61	61	8.11-94.73	0.1-84.4	1903-2016

(continued)

site	species code	all		with DBH		DBH range		date range
		n trees	n cores	n trees	n cores	sampled	reconstructed*	
SCBI	FRNI	12	12	12	12	11.04-39.2	0.5-27.3	1903-1996
SCBI	JUNI	30	30	28	28	20.4-76.19	5.6-59.5	1903-2010
SCBI	LITU	106	106	104	104	10-91.42	0.1-81.1	1903-2010
SCBI	PIST	36	36	36	36	13.92-50.96	0.5-44.3	1931-2010
SCBI	QUAL	66	66	66	66	11.4-76.73	0.3-70.4	1903-2009
SCBI	QUMO	67	67	67	67	10.22-84.59	0.3-69.5	1903-2017
SCBI	QURU	70	70	70	70	11.07-87.65	2.5-79.2	1903-2016
SCBI	QUVE	81	81	81	81	16.02-82.33	0.5-78.4	1903-2009
SC	PIMA	442	442	101	101	7-14.9	0.5-12.5	1903-2013
ZOF	ABAL	46	46	41	41	50-121	21.1-107.4	1903-2010
ZOF	FASY	1369	1369	1358	1358	unknown	0.1-115.3	1903-2013
ZOF	PCAB	644	644	599	599	unknown	0.5-126.4	1903-2011

*Maximum reconstructed *DBH*'s analyzed are less than maximum sampled *DBH*'s because we discard size ranges with < 3 conspecific trees.

Table S4. Allometric equations for bark thickness.

species	equation	source	n	DBH.range.cm	site	source.1
<i>Abies alba</i>	$bark.mm = ((0.05 + 0.06 * (dbh.cm/2.54))/2) * 2.54$	equation	NA		North America	Miles, Patrick D.; Smith, W. Brad. 2009.
<i>Acer pseudoplatanus</i>	$bark.mm = (0.619 * log(dbh.cm + 1)$	data	10	8.2-39.6	SCBI	Anderson-Teixeira et al. (2015)
<i>Betula alleghaniensis</i>	$bark.mm = ((0.15 + 0.03 * (dbh.cm/2.54))/2) * 2.54$	equation	NA		North America	Miles, Patrick D.; Smith, W. Brad. 2009.
<i>Betula papyrifera</i>	$bark.mm = ((0.13 + 0.05 * (dbh.cm/2.54))/2) * 2.54$	equation	NA		North America	Miles, Patrick D.; Smith, W. Brad. 2009.
<i>Carya cordiformis</i>	$bark.mm = 0.793 * log(dbh.cm + 1)$	data	9	5.9-68.2	SCBI	Anderson-Teixeira et al. (2015)
<i>Carya glabra</i>	$bark.mm = 1.035 * log(dbh.cm + 1)$	data	8	19.1-78	SCBI	Anderson-Teixeira et al. (2015)
<i>Carya ovalis</i>	$bark.mm = 1.531 * log(dbh.cm + 1)$	data	8	6.4-63.1	SCBI	Anderson-Teixeira et al. (2015)
<i>Carya tomentosa</i>	$bark.mm = 1.105 * log(dbh.cm + 1)$	data	8	5-57.3	SCBI	Anderson-Teixeira et al. (2015)
<i>Fraxinus americana</i>	$bark.mm = 2.223 * log(dbh.cm + 1)$	data	9	6.1-94.2	SCBI	Anderson-Teixeira et al. (2015)
<i>Jacaranda copaia</i>	$bark.mm = 2.993 * log(dbh.cm + 1)$	data	5	45.6-75	Panama	Raquel Alfaro-Sánchez (unpublished data)
<i>Juglans nigra</i>	$bark.mm = 2.107 * log(dbh.cm + 1)$	data	9	13.6-85.4	SCBI	Anderson-Teixeira et al. (2015)
<i>Liriodendron tulipifera</i>	$bark.mm = 1.637 * log(dbh.cm + 1)$	data	9	27.5-136.5	SCBI	Anderson-Teixeira et al. (2015)
<i>Picea abies</i>	$bark.mm = ((0.15 + 0.04 * (dbh.cm/2.54))/2) * 2.54$	equation	NA		North America	Miles, Patrick D.; Smith, W. Brad. 2009.
<i>Picea mariana</i>	$bark.mm = 3.726 * log(dbh.cm + 1)$	data	12	6.9-7.9	Scoty Creek	Rajit Pataankar and Jennifer Baltzer (unpublished data)
<i>Pinus flexilis</i>	$bark.mm = (1.299 * \sqrt{dbh.cm})^{0.699}^2$	equation	29	10-130	California (3 montane sites)	Zeibig-Kichas et al. (2016)
<i>Pinus ponderosa</i>	$bark.mm = (1.298 * \sqrt{dbh.cm})^{0.892}^2$	equation	81	5-160	California (4 montane sites)	Zeibig-Kichas et al. (2016)
<i>Pinus strobus</i>	$bark.mm = ((0.02 + 0.10 * (dbh.cm/2.54))/2) * 2.54$	equation	NA		North America	Miles, Patrick D.; Smith, W. Brad. 2009.
<i>Populus tremuloides</i>	$bark.mm = ((0.10 + 0.07 * (dbh.cm/2.54))/2) * 2.54$	equation	NA		North America	Miles, Patrick D.; Smith, W. Brad. 2009.
<i>Pseudotsuga menziesii</i>	$bark.mm = (0.785 * \sqrt{dbh.cm})^2$	equation	30	10-200	California (3 montane sites)	Zeibig-Kichas et al. (2016)
<i>Quercus alba</i>	$bark.mm = 1.828 * log(dbh.cm + 1)$	data	10	9.3-101.8	SCBI	Anderson-Teixeira et al. (2015)
<i>Quercus montana</i>	$bark.mm = 2.083 * log(dbh.cm + 1)$	data	8	5.8-99.1	SCBI	Anderson-Teixeira et al. (2015)
<i>Quercus rubra</i>	$bark.mm = 0.98 * log(dbh.cm + 1)$	data	10	24.1-143.2	SCBI	Anderson-Teixeira et al. (2015)
<i>Quercus velutina</i>	$bark.mm = 1.294 * log(dbh.cm + 1)$	data	8	16.2-210.7	SCBI	Anderson-Teixeira et al. (2015)
<i>Tetragastris panamensis</i>	$bark.mm = 1.672 * log(dbh.cm + 1)$	data	4	22.7-48.8	Panama	Raquel Alfaro-Sánchez (unpublished data)
<i>Trichilia tuberculata</i>	$bark.mm = 1.367 * log(dbh.cm + 1)$	data	12	21-40.5	Panama	Raquel Alfaro-Sánchez (unpublished data), Pete Kerby-Miller and Helene Muller-Landau (unpublished data)
<i>Tsuga canadensis</i>	$bark.mm = ((0.18 + 0.08 * (dbh.cm/2.54))/2) * 2.54$	equation	NA		North America	Miles, Patrick D.; Smith, W. Brad. 2009.

For assignments of species as proxies for those without available bark allometries, see Table S2.

Table S5. Qualitative comparison of results from this study with previous studies employing conventional methods.

species	Precipitation response		Temperature response		reference
	previously observed	observed here	previously observed	observed here	
Barro Colorado Island, Panama					
JACO	pos. correlation to Apr-Dec <i>PPT</i> (strongest of the 3 species)	pos. correlation to Mar-Dec <i>PPT</i> (strongest of the 3 species)	no sig. correlation to annual T_{mean} or T_{min}	neg. response to Feb-Mar T_{min}	Alfaro-Sánchez et al. 2017
TEPA	pos. correlation to Apr-Dec <i>PPT</i> (response weaker than JACO, similar to TRTU)	pos. correlation to Mar-Dec <i>PPT</i> (response weaker than JACO, similar to TRTU)	no sig. correlation to annual T_{mean} or T_{min}	no sig. correlation to Feb-Mar T_{min}	Alfaro-Sánchez et al. 2017
TRTU	pos. correlation to Apr-Dec <i>PPT</i> (response weaker than JACO, similar to TEPA)	pos. correlation to Mar-Dec <i>PPT</i> (response weaker than JACO, similar to TEPA)	no sig. correlation to annual T_{mean} or T_{min}	non-sig. slight pos. response to Feb-Mar T_{min}	Alfaro-Sánchez et al. 2017
Huai Kha Khaeng, Thailand					
AFXY	sig. pos. correlation with June <i>PPT</i> , otherwise n.s.	slight concave-down response to p.Sept-June <i>PPT</i> frequency	sig. neg. correlation with T_{max} in Aug and Dec; T_{min} in p.Oct., Jul, Aug	slight concave-down response to Apr-Oct T_{max}	Vlam et al. 2013
CHTA	sig. pos. correlation with April <i>PPT</i> , otherwise n.s.	slight concave-down response to p.Sept-June <i>PPT</i> frequency	sig. neg. correlation with T_{max} in May, Aug-Sept; T_{min} in Feb, May, Aug	slight neg. response to Apr-Oct T_{max}	Vlam et al. 2013
MEAZ	sig. pos. correlation with April <i>PPT</i> , otherwise n.s.	concave-down response to p.Sept-June <i>PPT</i> frequency	sig. neg. correlation with T_{max} in May-Aug; T_{min} in May-Aug	neg. response to Apr-Oct T_{max}	Vlam et al. 2013
TOCI	sig. pos. correlation with p.Oct-p.Nov and April-May <i>PPT</i>	concave-down /increasing response to p.Sept-June <i>PPT</i> frequency	sig. neg. correlation with T_{max} every month from pOct-June (excluding March); T_{min} in Jan and Mar-Aug	neg. response to Apr-Oct T_{max}	Vlam et al. 2013
Smithsonian Conservation Biology Institute, Virginia, USA					
CACO	pos. correlations with May-Aug <i>PPT</i> (sig. May, July)	neg. correlations with May-Aug <i>PET</i> (sig. May-July)	**(sig or ns)** neg. response to May-July <i>PET</i>	Helcoski et al. 2019	
CAGL	pos. correlations with May-Aug <i>PPT</i> (sig. May)	neg. correlations with May-Aug <i>PET</i> (n.s.)	**(sig or ns)** neg. response to May-July <i>PET</i>	Helcoski et al. 2019	
CAOVL	pos. correlations with May-Aug <i>PPT</i> (sig. Aug)	neg. correlations with May-Aug <i>PET</i> (sig. all months)	**(sig or ns)** neg. response to May-July <i>PET</i>	Helcoski et al. 2019	
CATO	pos. correlations with May-Aug <i>PPT</i> (n.s.)	neg. correlations with May-Aug <i>PET</i> (sig. June)	**(sig or ns)** neg. response to May-July <i>PET</i>	Helcoski et al. 2019	
FAGR	pos. correlations with May-Aug <i>PPT</i> (sig. July-Aug)	neg. correlations with May-Aug <i>PET</i> (sig. July-Aug)	**(sig or ns)** neg. response to May-July <i>PET</i>	Helcoski et al. 2019	
FRAM	pos. correlations with May-Aug <i>PPT</i> (sig. May-June)	neg. correlations with May-Aug <i>PET</i> (sig. May-June)	**(sig or ns)** neg. response to May-July <i>PET</i>	Helcoski et al. 2019	
FRNI	no sig. correlations with peak growing season <i>PPT</i>	no sig. correlations with peak growing season <i>PET</i>	**(sig or ns)** neg. response to May-July <i>PET</i>	Helcoski et al. 2019	
JUNI	pos. correlations with May-Aug <i>PPT</i> (sig. Jun-Aug)	neg. correlations with May-Aug <i>PET</i> (sig. July-Aug)	non-sig. neg. response to May-July <i>PET</i>	Helcoski et al. 2019	

S5, cont.

species	Precipitation response		Temperature response		reference
	previously observed	observed here	previously observed	observed here	
Smithsonian Conservation Biology Institute, Virginia, USA (cont.)					
LITU	pos. correlations with May-Aug <i>PPT</i> (sig. May-July)		neg. correlations with May-Aug <i>PET</i> (sig. all months)	**(sig or ns)** neg. response to May-July <i>PET</i>	Helcoski et al. 2019
PIST	pos. correlations with May-Aug <i>PPT</i> (n.s.)		neg. correlations with May-Aug <i>PET</i> (n.s.)	**(sig or ns)** neg. response to May-July <i>PET</i>	Helcoski et al. 2019
QUAL	pos. correlations with May-Aug <i>PPT</i> (sig. May)		neg. correlations with May-Aug <i>PET</i> (sig. all months)	**(sig or ns)** neg. response to May-July <i>PET</i>	Helcoski et al. 2019
QUMO	pos. correlations with May-Aug <i>PPT</i> (sig. May)		neg. correlations with May-Aug <i>PET</i> (sig. May-June, Aug)	**(sig or ns)** neg. response to May-July <i>PET</i>	Helcoski et al. 2019
QURU	pos. correlations with May-Aug <i>PPT</i> (n.s.)		neg. correlations with May-Aug <i>PET</i> (sig. May, July-Aug)	**(sig or ns)** neg. response to May-July <i>PET</i>	Helcoski et al. 2019
QUVE	pos. correlations with May-Aug <i>PPT</i> (sig. May-July)		neg. correlations with May-Aug <i>PET</i> (sig. all months)	**(sig or ns)** neg. response to May-July <i>PET</i>	Helcoski et al. 2019
Lilly Dickey Woods, Indiana, USA					
LITU	pos. correlations with Jun-Aug PDSI	pos. response to June <i>PPT</i>	neg. response to Jun-Aug <i>T_{max}</i>	neg. response to June <i>PET</i>	Maxwell, Harley, and Robeson 2016
QUAL	pos. correlations with Jun-Aug PDSI	pos. response to June <i>PPT</i>	neg. response to Jun-Aug <i>T_{max}</i>	neg. response to June <i>PET</i>	Maxwell, Harley, and Robeson 2016
QUMO	pos. correlations with Jun-Aug PDSI	pos. response to June <i>PPT</i>	neg. response to Jun-Aug <i>T_{max}</i>	neg. response to June <i>PET</i>	Maxwell, Harley, and Robeson 2016
QUVE	pos. correlations with Jun-Aug PDSI	pos. response to June <i>PPT</i>	neg. response to Jun-Aug <i>T_{max}</i>	neg. response to June <i>PET</i>	Maxwell, Harley, and Robeson 2016
Harvard Forest, Massachusetts, USA					
ACRU			no response to Jan- April <i>T_{min}</i> *	neg. correlation to Mar <i>PET</i>	Alexander et al. 2019
BEAL			no response to Jan- April <i>T_{min}</i> *	ns neg correlation with Mar <i>PET</i>	Alexander et al. 2019
QURU			no response to Jan- April <i>T_{min}</i> *	slight concave-down decreasing response to Mar <i>PET</i>	Alexander et al. 2019
TSCA			pos. response to Jan- April <i>T_{min}</i> *	pos. response to March <i>PET</i>	Alexander et al. 2019

S5, cont.

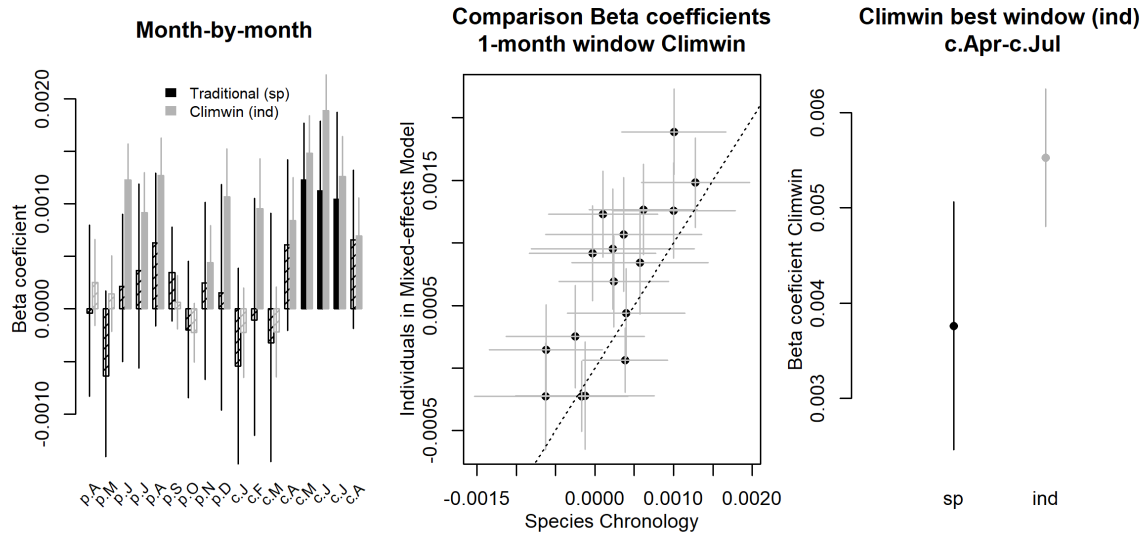
species	Precipitation response		Temperature response		reference
	previously observed	observed here	previously observed	observed here	
Žofín Forest Dynamics Plot, Czech Republic					
ABAL	no sig. correlations with June-July <i>PPT</i>	slight concave-down response to p.Jun-p.July <i>PPT</i> frequency	sig. pos. correlation to April T (strongest T correlation)	pos. response to Jan-March <i>T_{max}</i>	Kašpar, Tumajer, Vašíčková, and Šamonil, in review
FASY	no sig. correlations with June-July <i>PPT</i>	pos. response to p.Jun-p.July <i>PPT</i> frequency	sig. pos. correlation to Jan T (strongest T correlation)	pos. response to Jan-March <i>T_{max}</i>	Kašpar, Tumajer, Vašíčková, and Šamonil, in review
PIAB	modest pos. correlations (n.s) with June-July <i>PPT</i> ≥700m elev. sites moisture limited June-Aug	pos. response to p.Jun-p.July <i>PPT</i> frequency	sig. pos. correlation to March T (strongest current-year T correlation) ≥700m elev. sites temperature limited except June-Aug	pos. response to Jan-March <i>T_{max}</i>	Kašpar, Tumajer, Vašíčková, and Šamonil, in review Tumajer et al. 2017
Niobrara and Hansley, Nebraska, USA					
BEPA	little relationship to ppt within analysis timeframe (exception: pos. corr. with pAug pre); stronger relationship to streamflow and PDSI		little relationship to <i>T_{mean}</i> within analysis timeframe (exception: neg. corr. with pJune and cJan <i>T_{mean}</i>)		Bumann et al. 2019
JUVI	pos. correlations with <i>PPT</i> pJul-cJune		neg. correlation to cJun-cJul <i>T_{mean}</i>		Aus de Ar et al. 2018
PIPO	pos. correlations with <i>PPT</i> cApr-cAug		neg. correlation to <i>T_{mean}</i> in pJul, pSep, cMay, cJul		Aus de Ar et al. 2018
PIPO					Touchan et al., 2011 and Williams et al., 2013 Touchan et al., 2011 and Williams et al., 2013 -
PIST2					Sniderhan and Baltzer 2016

*Indicates results from a regional study including but not limited to cores from the focal site.

**Indicates results from a regional study not including the focal site, but believed to be representative.

Figure S1. Comparison of our approach with traditional methods of identifying climate signals: LITU at SCBI.

Precipitation



Potential Evapotranspiration

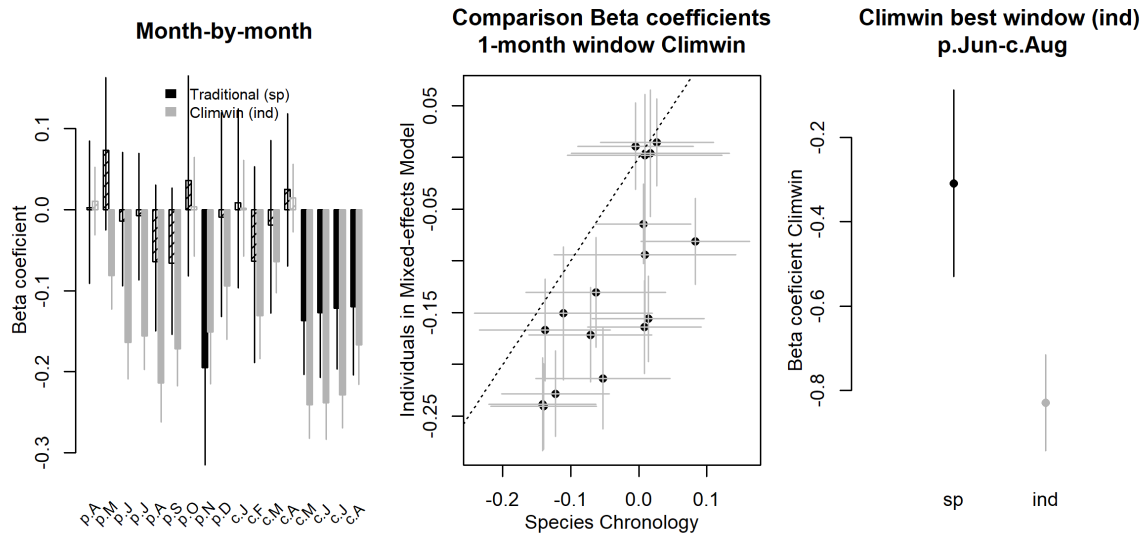
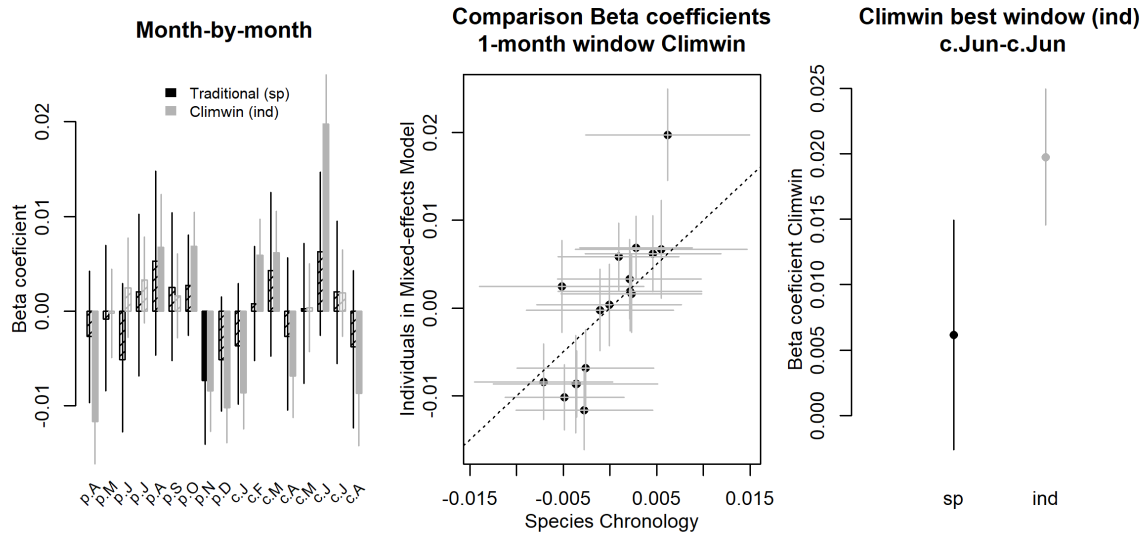


Figure S1. Comparison of our approach with traditional methods of identifying climate signals: LITU at SCBI. Shown are responses to the precipitation- and temperature-group variables selected as most influential by the *climwin* analysis. Left panels show a month-by-month comparison of *beta* (slope) coefficients for the relationship between tree growth and the monthly climate variable from species-level residual chronologies (traditional approach) and from individual-level analysis in *climwin* (approach presented here). Center panels compare the monthly *beta* coefficient estimates, with the dotted line indicating 1:1 correspondence. Finally, the right panels compare *beta* coefficients for the optimal window selected by *climwin*. Error bars indicate standard error of slope estimates. Note that 1:1 correspondence is not necessarily expected. See Appendix 5 for analysis methods and discussion of expected correspondence.

Figure S2. Comparison of our approach with traditional methods of identifying climate signals: ABAL at Zofin.

Precipitation Day Frequency



Maximum temperature

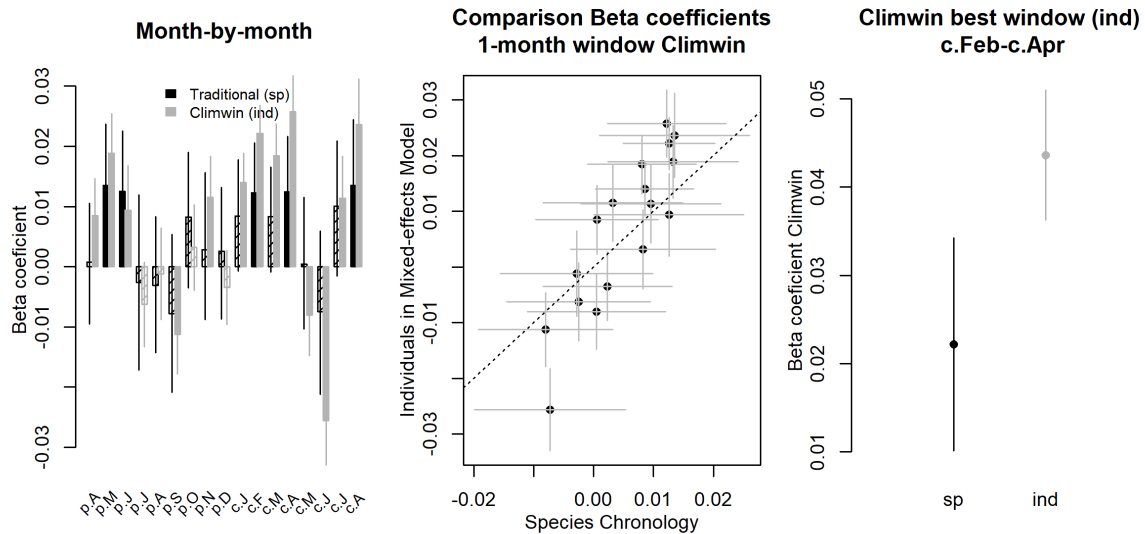
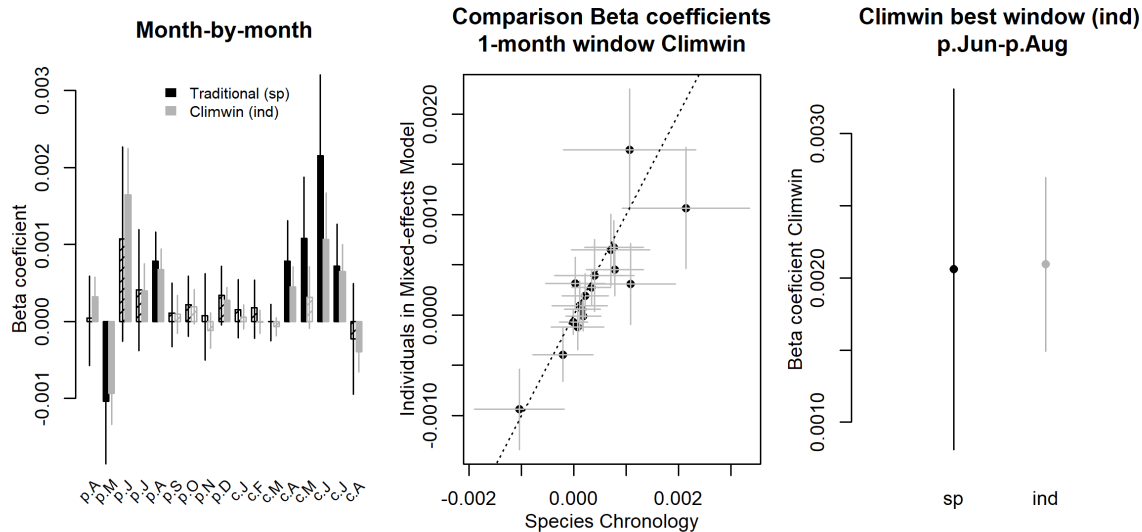


Figure S2. Comparison of our approach with traditional methods of identifying climate signals: ABAL at Zofin. Shown are responses to the precipitation- and temperature-group variables selected as most influential by the *climwin* analysis. Left panels show a month-by-month comparison of *beta* (slope) coefficients for the relationship between tree growth and the monthly climate variable from species-level residual chronologies (traditional approach) and from individual-level analysis in *climwin* (approach presented here). Center panels compare the monthly *beta* coefficient estimates, with the dotted line indicating 1:1 correspondence. Finally, the right panels compare *beta* coefficients for the optimal window selected by *climwin*. Error bars indicate standard error of slope estimates. Note that 1:1 correspondence is not necessarily expected. See Appendix 5 for analysis methods and discussion of expected correspondence.

Figure S3. Comparison of our approach with traditional methods of identifying climate signals: PSME at Cedar Breaks.

Precipitation



Maximum temperature

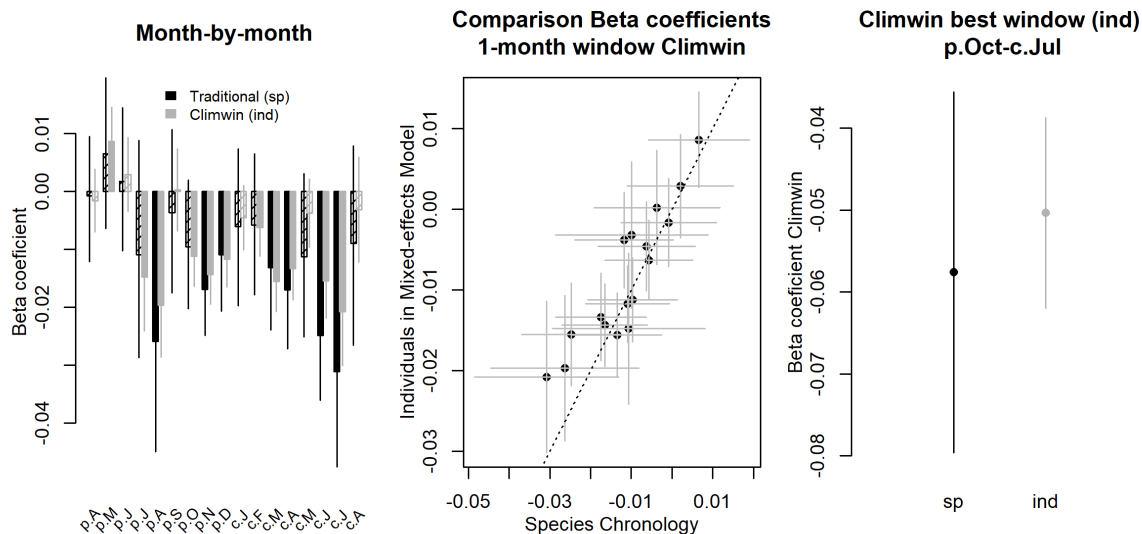
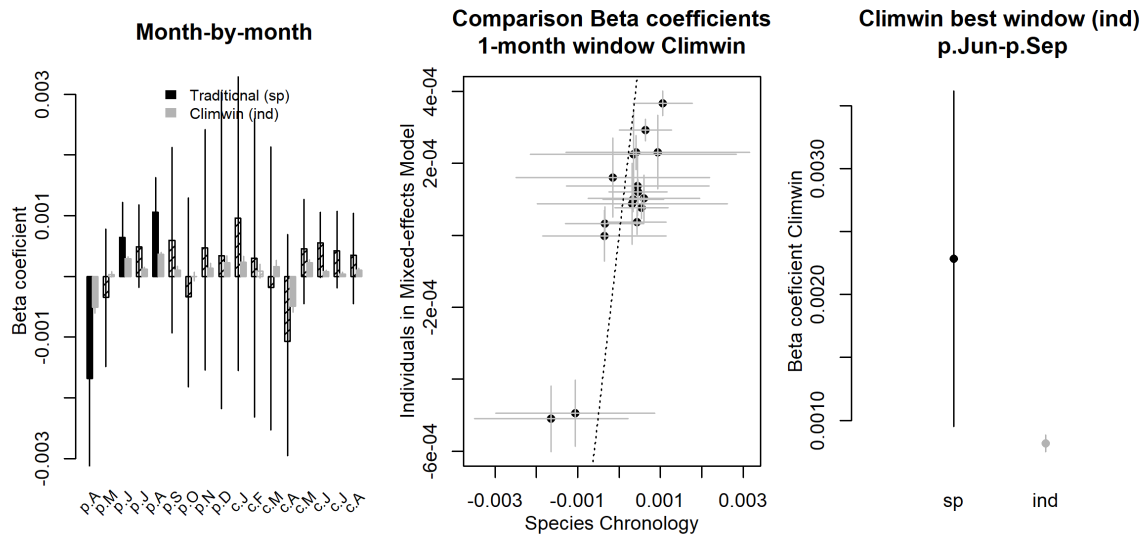


Figure S3. Comparison of our approach with traditional methods of identifying climate signals: PSME at Cedar Breaks. Shown are responses to the precipitation- and temperature-group variables selected as most influential by the *climwin* analysis. Left panels show a month-by-month comparison of *beta* (slope) coefficients for the relationship between tree growth and the monthly climate variable from species-level residual chronologies (traditional approach) and from individual-level analysis in *climwin* (approach presented here). Center panels compare the monthly *beta* coefficient estimates, with the dotted line indicating 1:1 correspondence. Finally, the right panels compare *beta* coefficients for the optimal window selected by *climwin*. Error bars indicate standard error of slope estimates. Note that 1:1 correspondence is not necessarily expected. See Appendix 5 for analysis methods and discussion of expected correspondence.

Figure S4. Comparison of our approach with traditional methods of identifying climate signals: PIMA at Scotty Creek.

Precipitation



Maximum temperature

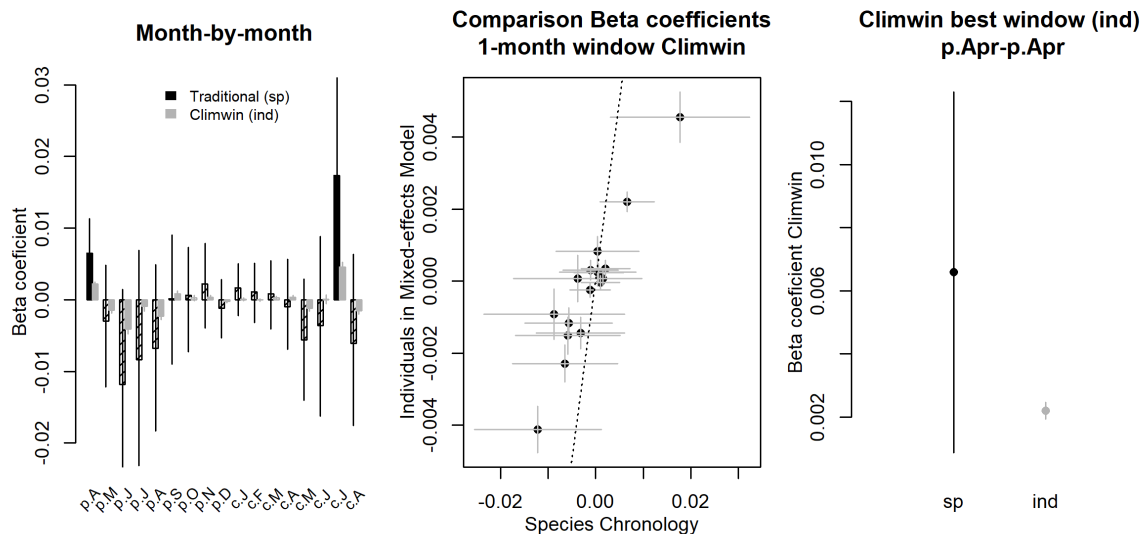


Figure S4. Comparison of our approach with traditional methods of identifying climate signals: PIMA at Scotty Creek. Shown are responses to the precipitation- and temperature-group variables selected as most influential by the *climwin* analysis. Left panels show a month-by-month comparison of *beta* (slope) coefficients for the relationship between tree growth and the monthly climate variable from species-level residual chronologies (traditional approach) and from individual-level analysis in *climwin* (approach presented here). Center panels compare the monthly *beta* coefficient estimates, with the dotted line indicating 1:1 correspondence. Finally, the right panels compare *beta* coefficients for the optimal window selected by *climwin*. Error bars indicate standard error of slope estimates. Note that 1:1 correspondence is not necessarily expected. See Appendix 5 for analysis methods and discussion of expected correspondence.

Figure S5. (PRE at SCBI)

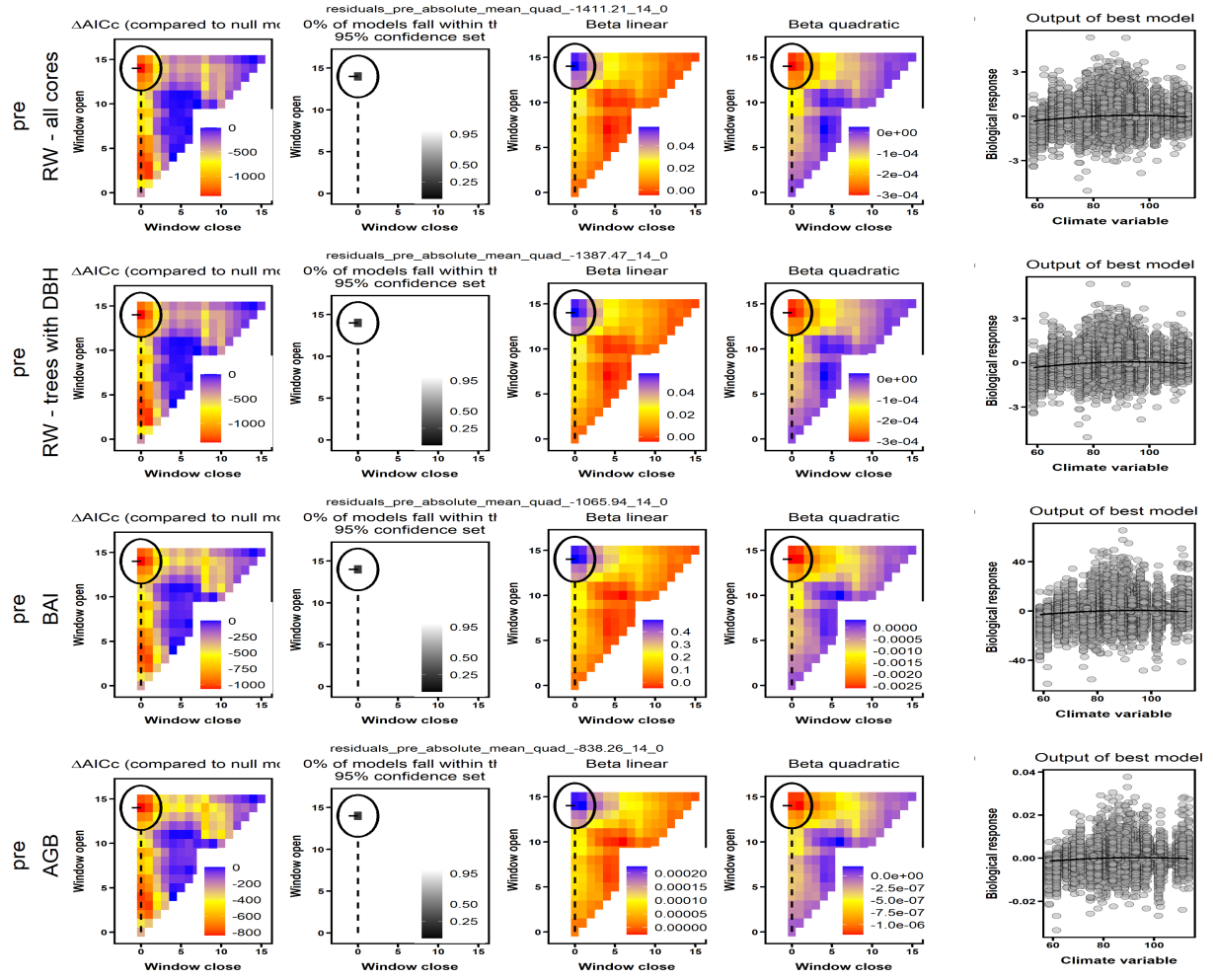


Figure S5. (PRE at SCBI) Here, *climwin* identified **GIVE WINDOW** precipitation (*PPT*) as the strongest climate variable across all four analyses (*RW* with and without trees for which *DBH* could not be reconstructed, *BAI*, ΔAGB).

Figure S6. (PET at SCBI)

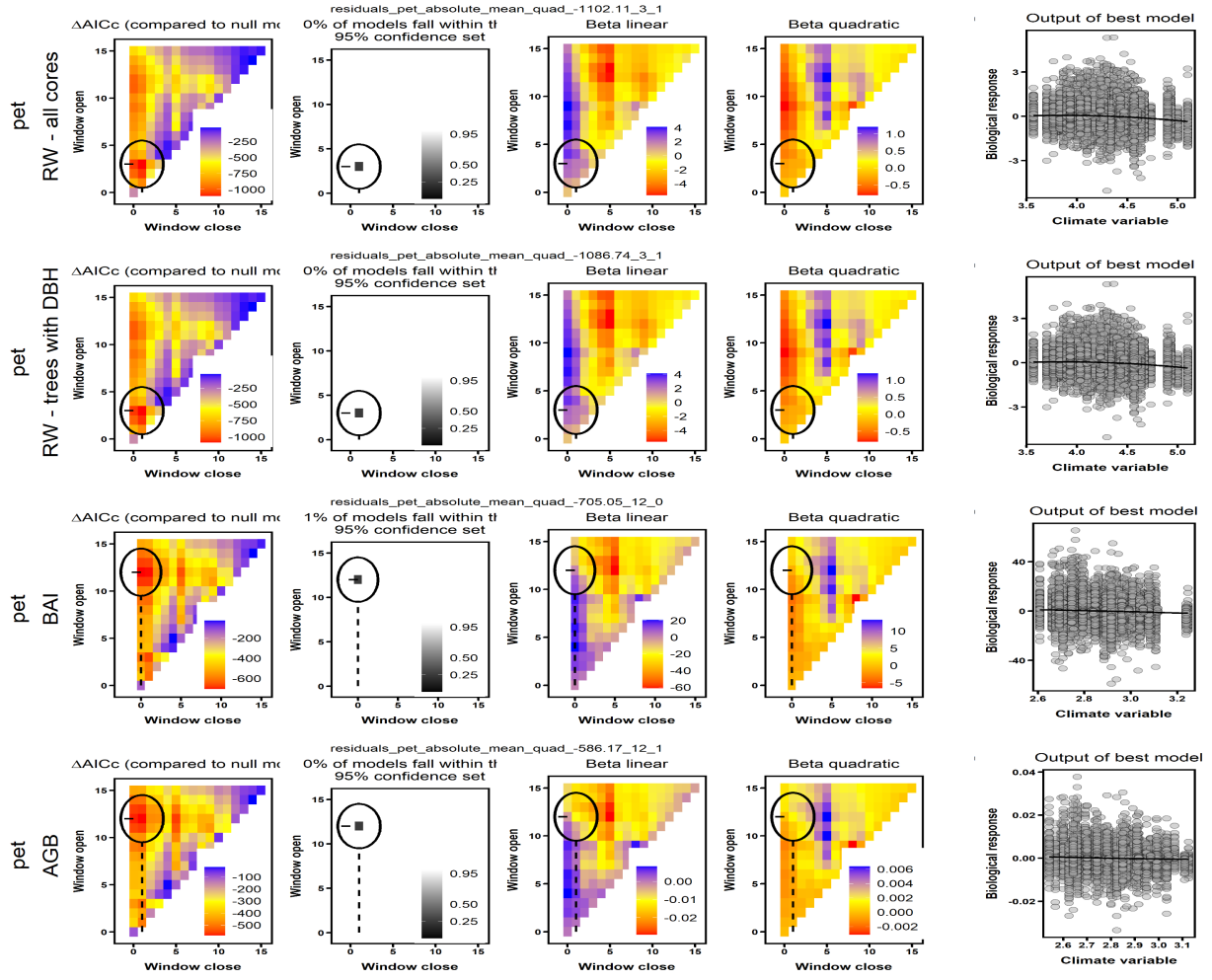


Figure S6. (PET at SCBI) Here, *climwin* identified potential evapotranspiration (PET) as the strongest climate variable across all four analyses (*RW* with and without trees for which *DBH* could not be reconstructed, *BAI*, ΔAGB), but a different window (**GIVE WINDOW**) was chosen for *BAI* and ΔAGB than for *RW* (**GIVE WINDOW**).

Figure S7. (TMX/TMP at HKK)

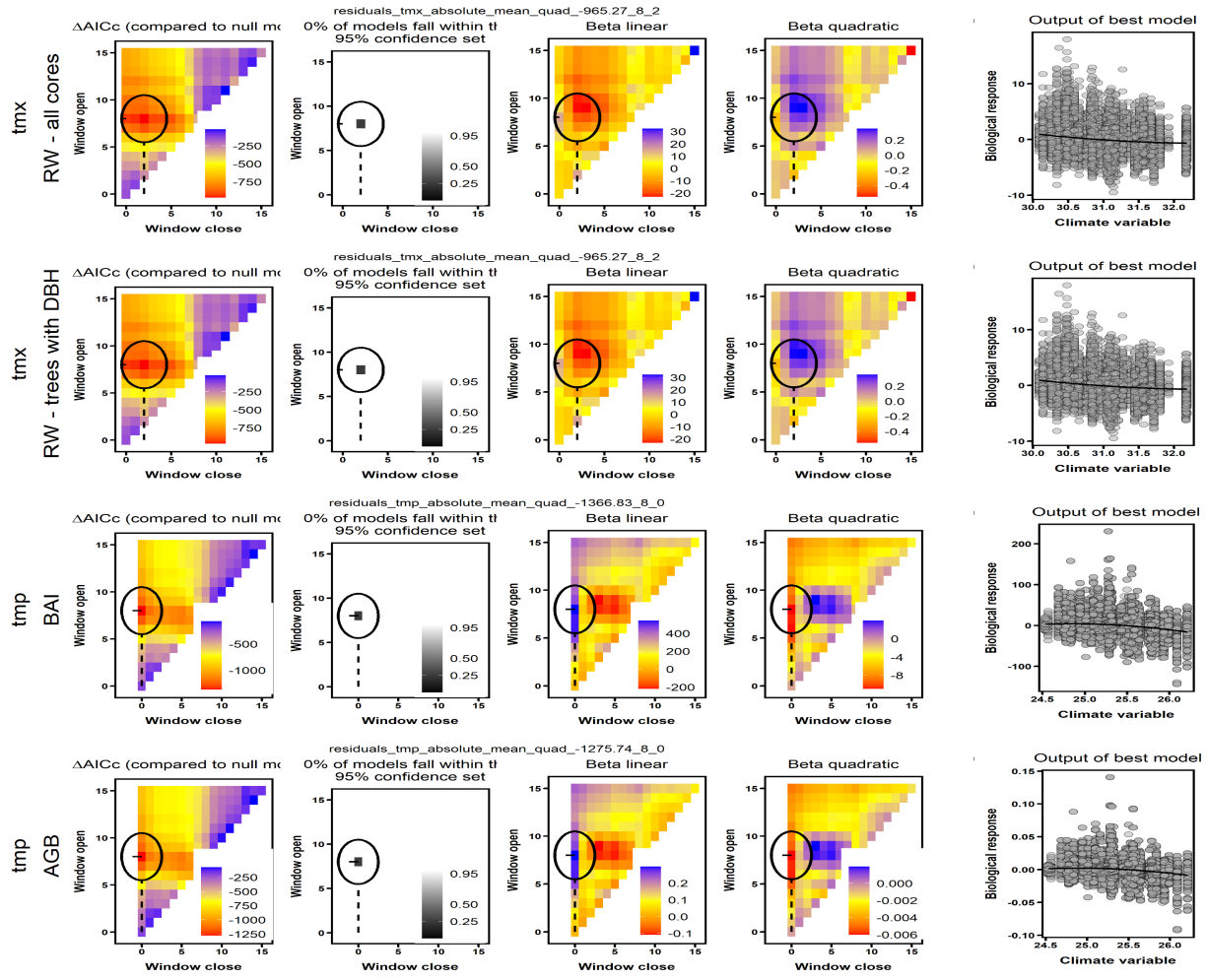


Figure S7. (TMX/TMP at HKK) Here....

Figure S9. Best GLS models for Barro Colorado Island (Panama)

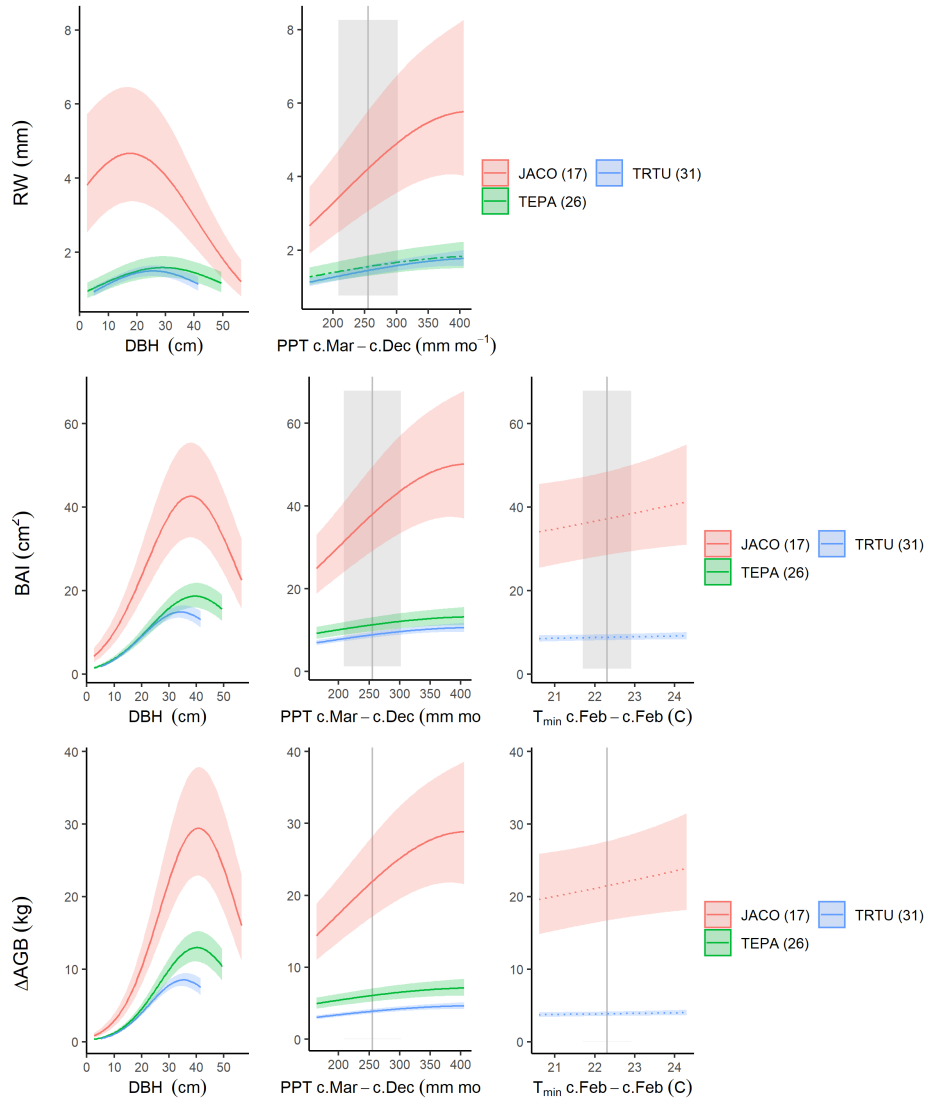


Figure S9. Best GLS models for Barro Colorado Island (Panama) for all three growth metrics examined here. Precipitation and temperature group variables are as selected by *climwin* (*p*=previous year, *c*=current year). For each species, relationships are plotted if included in top model, with best-fit polynomials plotted with solid lines when both first- and second-order terms are significant, dashed lines when only one term is significant, and dotted lines when neither is significant. Transparent ribbons indicate 95% confidence intervals. Vertical grey lines indicate the long-term mean for the climate variable, shading indicates 1 SD.

Figure S10. Best GLS models for Huai Kha Khaeng (Thailand)

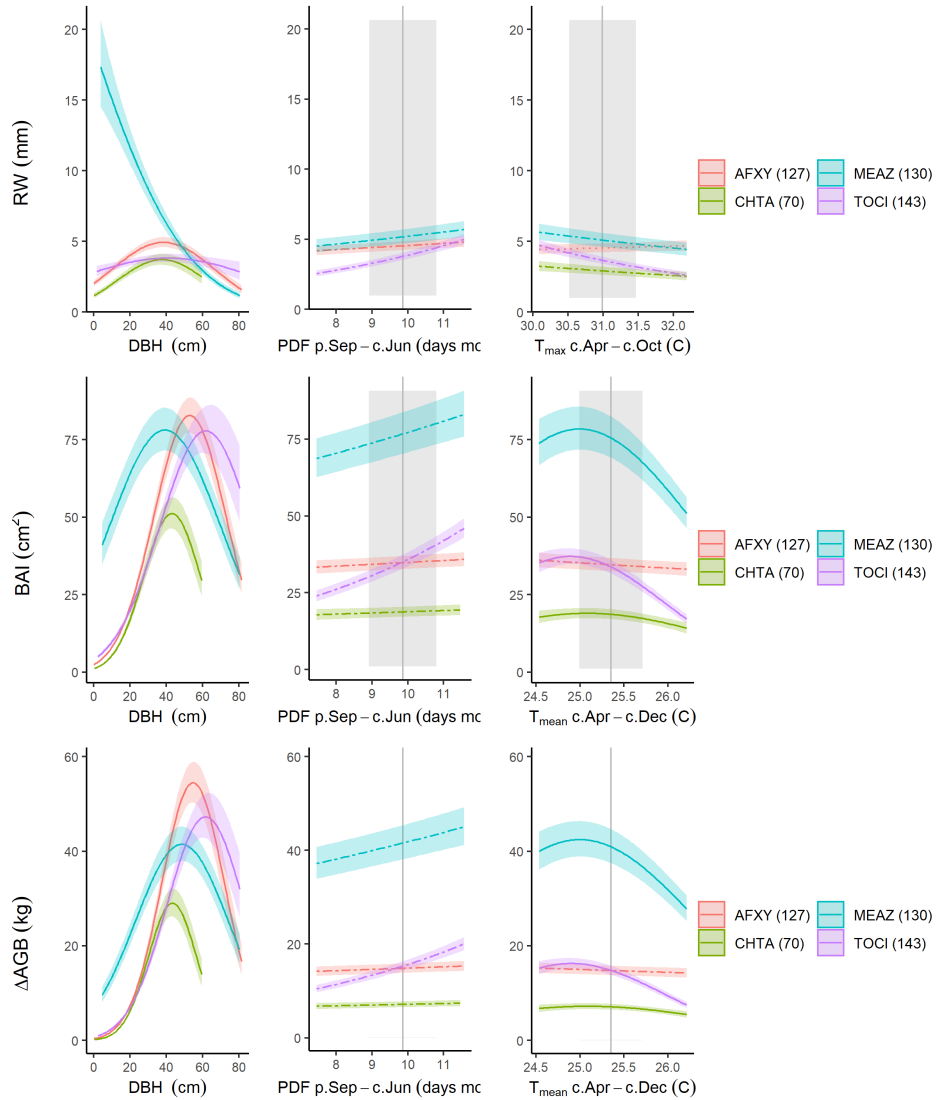


Figure S10. Best GLS models for Huai Kha Khaeng (Thailand) for all three growth metrics examined here. Precipitation and temperature group variables are as selected by *climwin* (*p*=previous year, *c*=current year). For each species, relationships are plotted if included in top model, with best-fit polynomials plotted with solid lines when both first- and second-order terms are significant, dashed lines when only one term is significant, and dotted lines when neither is significant. Transparent ribbons indicate 95% confidence intervals. Vertical grey lines indicate the long-term mean for the climate variable, shading indicates 1 SD.

Figure S11. Best GLS models for the Smithsonian Conservation Biology Institute (Virginia, USA)

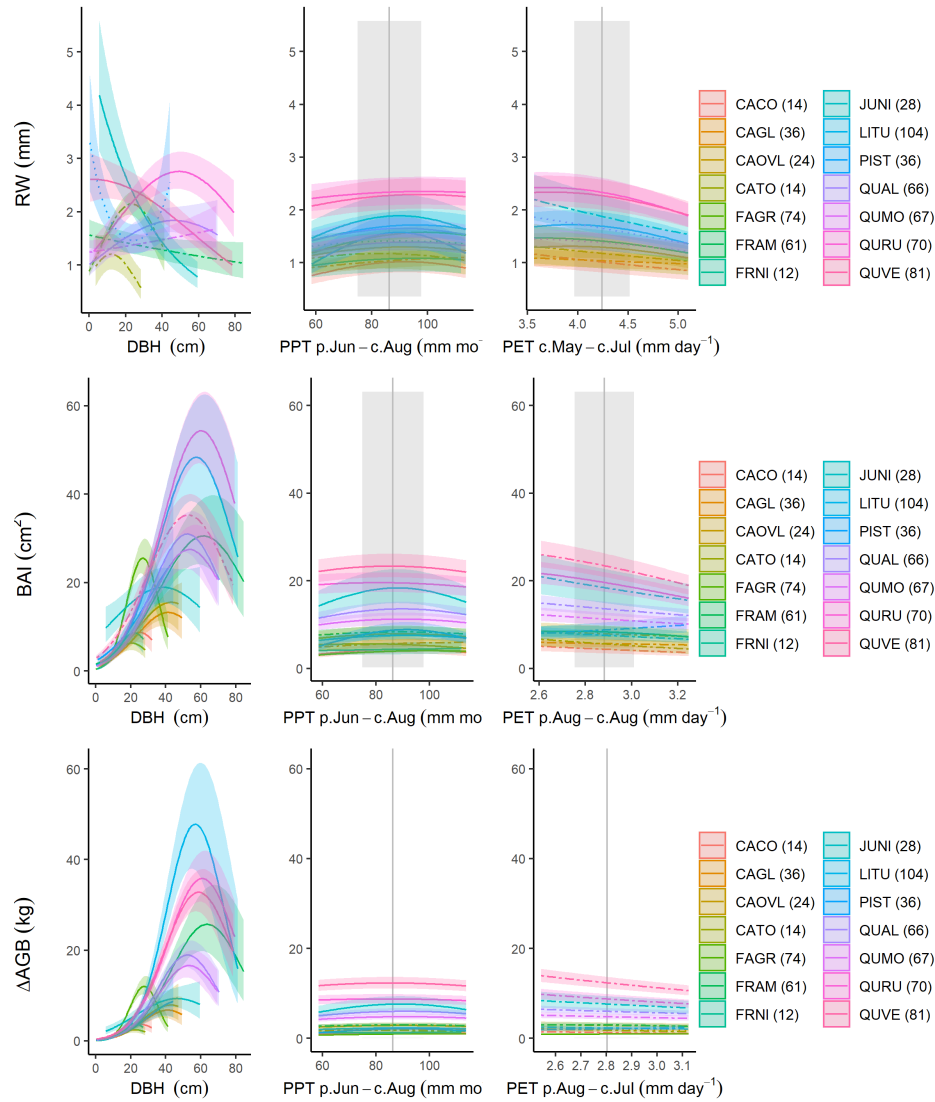


Figure S11. Best GLS models for the Smithsonian Conservation Biology Institute (Virginia, USA) for all three growth metrics examined here. Precipitation and temperature group variables are as selected by *climwin* (*p*=previous year, *c*=current year). For each species, relationships are plotted if included in top model, with best-fit polynomials plotted with solid lines when both first- and second-order terms are significant, dashed lines when only one term is significant, and dotted lines when neither is significant. Transparent ribbons indicate 95% confidence intervals. Vertical grey lines indicate the long-term mean for the climate variable, shading indicates 1 SD.

Figure S12. Best GLS models for Lilley Dickey Woods (Indiana, USA)

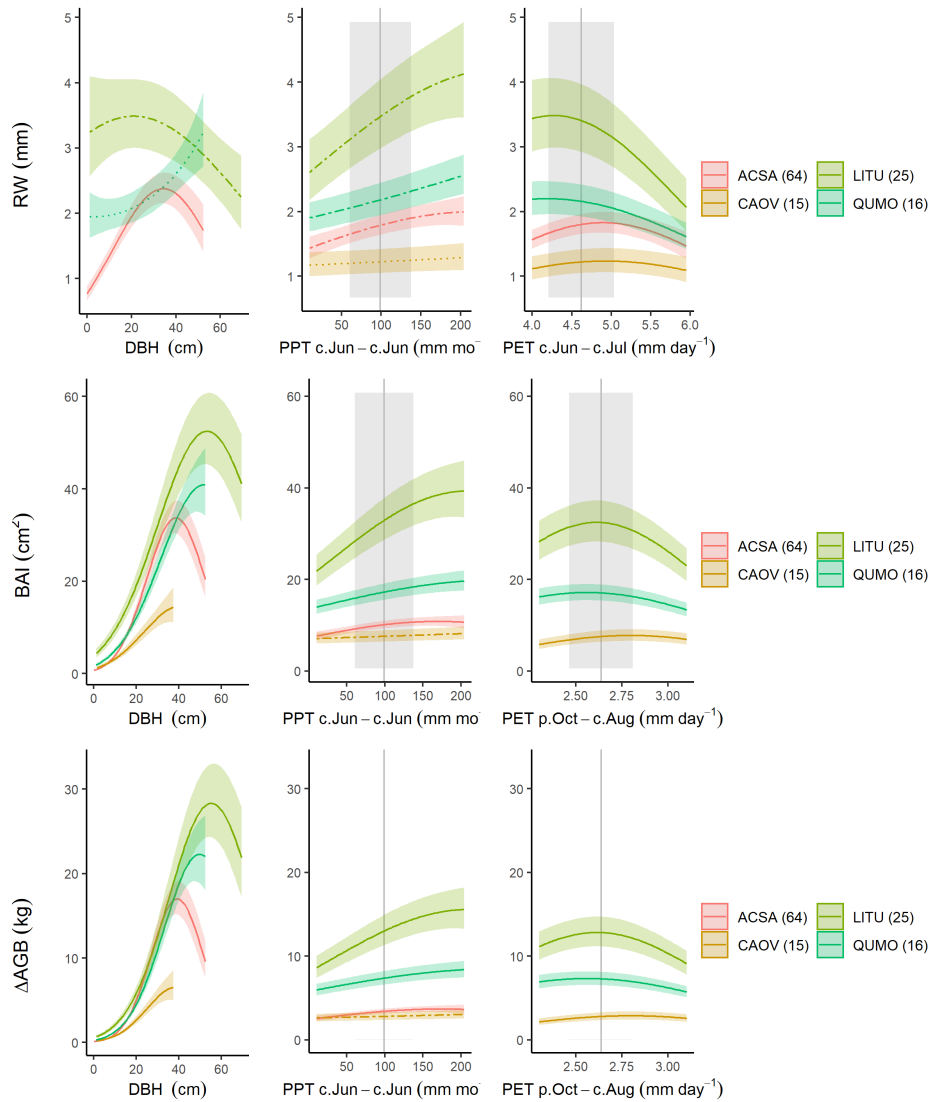


Figure S12. Best GLS models for Lilley Dickey Woods (Indiana, USA) for all three growth metrics examined here. Precipitation and temperature group variables are as selected by *climwin* (*p*=previous year, *c*=current year). For each species, relationships are plotted if included in top model, with best-fit polynomials plotted with solid lines when both first- and second-order terms are significant, dashed lines when only one term is significant, and dotted lines when neither is significant. Transparent ribbons indicate 95% confidence intervals. Vertical grey lines indicate the long-term mean for the climate variable, shading indicates 1 SD.

Figure S13. Best GLS models for Harvard Forest (Massachusetts, USA)

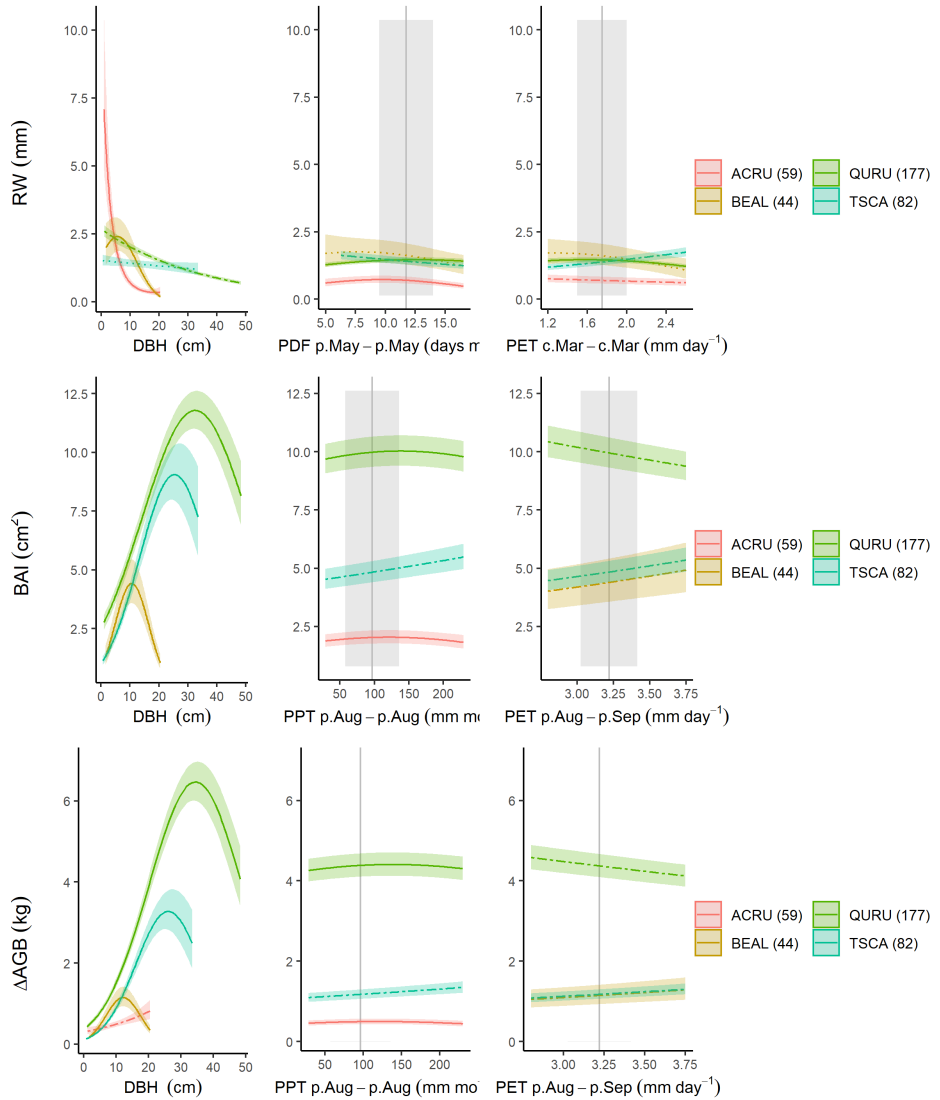


Figure S13. Best GLS models for Harvard Forest (Massachusetts, USA) for all three growth metrics examined here. Precipitation and temperature group variables are as selected by *climwin* (*p*=previous year, *c*=current year). For each species, relationships are plotted if included in top model, with best-fit polynomials plotted with solid lines when both first- and second-order terms are significant, dashed lines when only one term is significant, and dotted lines when neither is significant. Transparent ribbons indicate 95% confidence intervals. Vertical grey lines indicate the long-term mean for the climate variable, shading indicates 1 SD.

Figure S14. Best GLS models for Zofin Forest (Czech Republic)

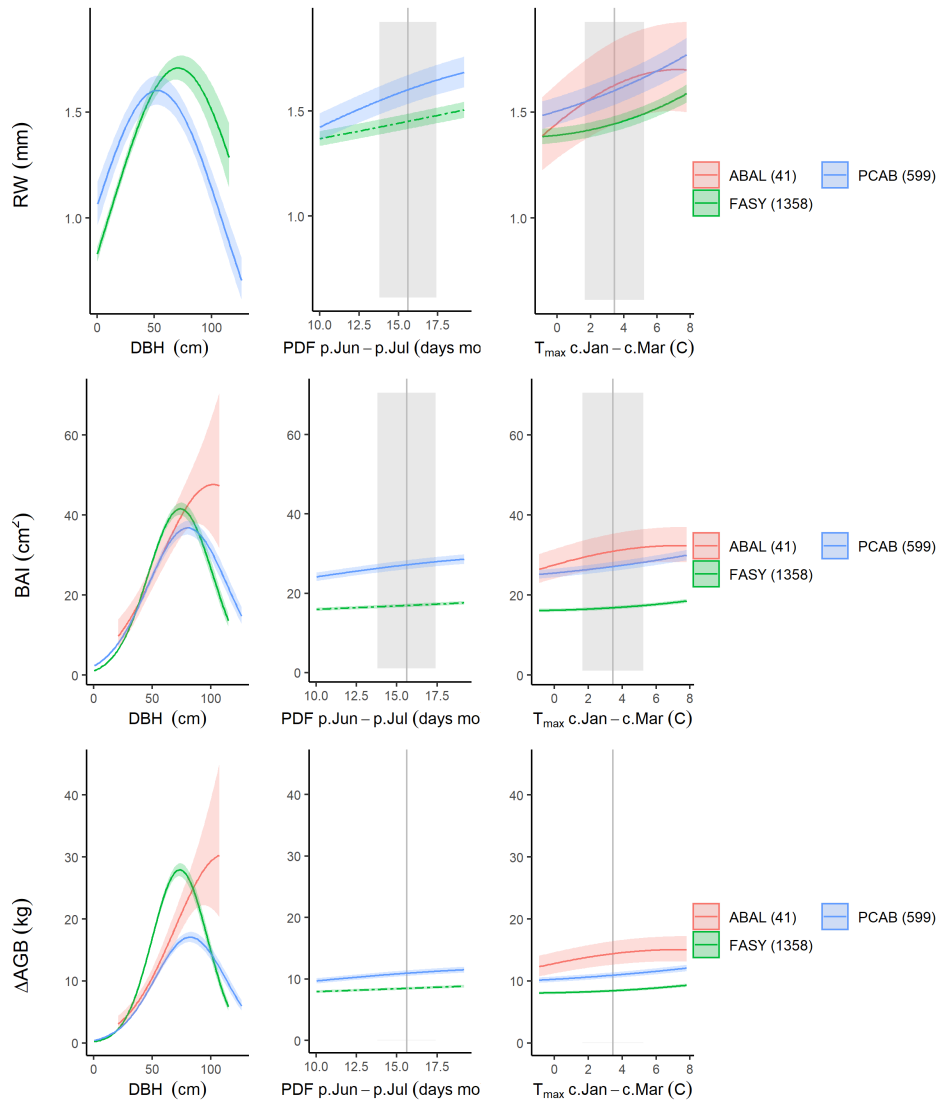


Figure S14. Best GLS models for Zofin Forest (Czech Republic) for all three growth metrics examined here. Precipitation and temperature group variables are as selected by *climwin* (p =previous year, c =current year). For each species, relationships are plotted if included in top model, with best-fit polynomials plotted with solid lines when both first- and second-order terms are significant, dashed lines when only one term is significant, and dotted lines when neither is significant. Transparent ribbons indicate 95% confidence intervals. Vertical grey lines indicate the long-term mean for the climate variable, shading indicates 1 SD.

Figure S15. Best GLS models for Niobrara/ Halsey (Nebraska, USA)

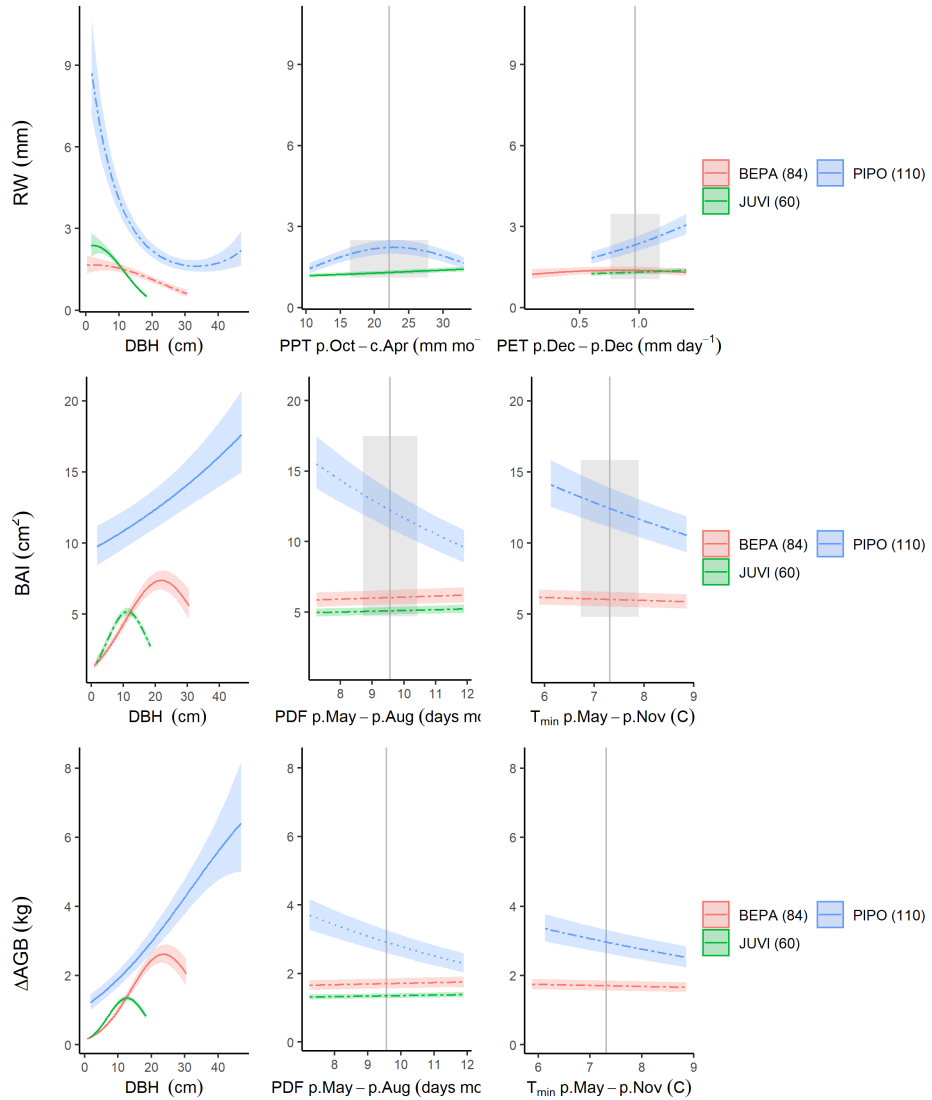


Figure S15. Best GLS models for Niobrara/ Halsey (Nebraska, USA) for all three growth metrics examined here. Precipitation and temperature group variables are as selected by *climwin* (*p*=previous year, *c*=current year). For each species, relationships are plotted if included in top model, with best-fit polynomials plotted with solid lines when both first- and second-order terms are significant, dashed lines when only one term is significant, and dotted lines when neither is significant. Transparent ribbons indicate 95% confidence intervals. Vertical grey lines indicate the long-term mean for the climate variable, shading indicates 1 SD.

Figure S16. Best GLS models for Little Tesuque (New Mexico, USA)

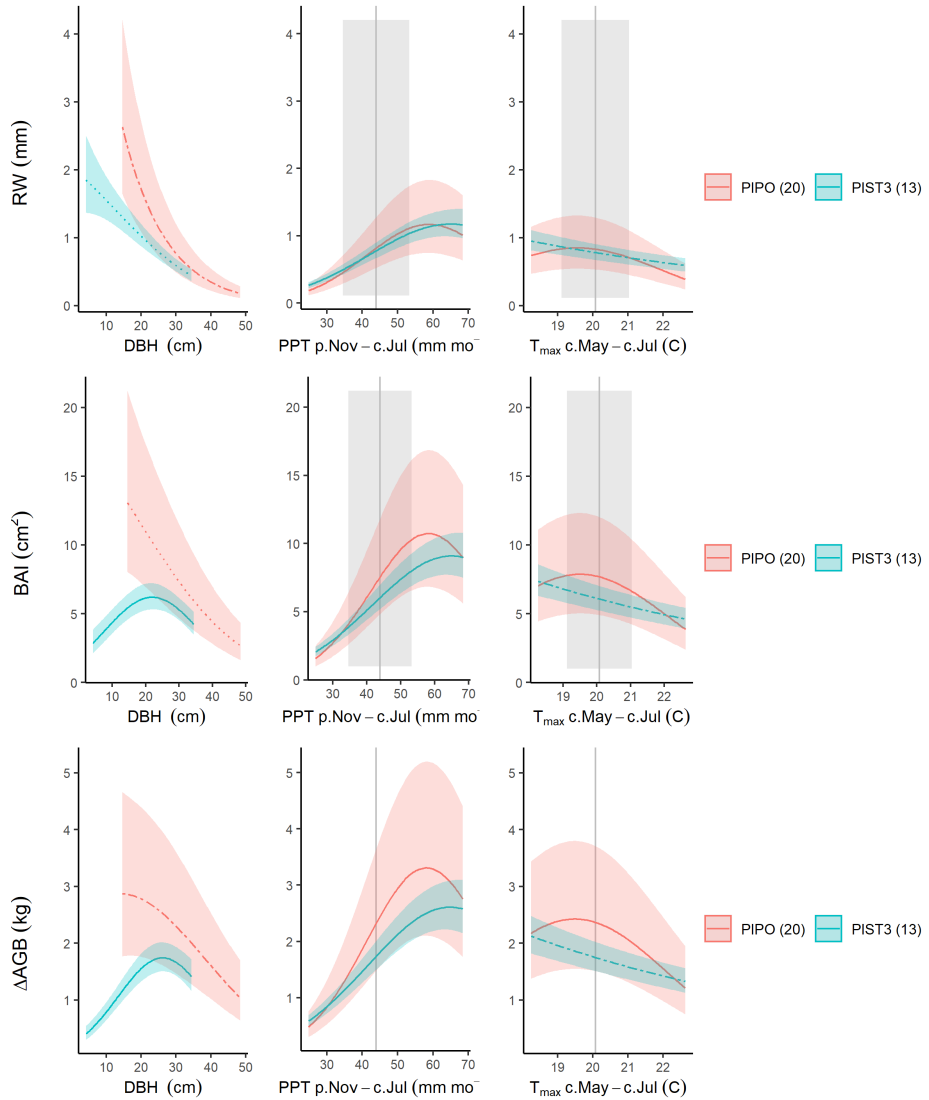


Figure S16. Best GLS models for Little Tesuque (New Mexico, USA) for all three growth metrics examined here. Precipitation and temperature group variables are as selected by *climwin* (*p*=previous year, *c*=current year). For each species, relationships are plotted if included in top model, with best-fit polynomials plotted with solid lines when both first- and second-order terms are significant, dashed lines when only one term is significant, and dotted lines when neither is significant. Transparent ribbons indicate 95% confidence intervals. Vertical grey lines indicate the long-term mean for the climate variable, shading indicates 1 SD.

Figure S17. Best GLS models for Cedar Breaks (Utah, USA)

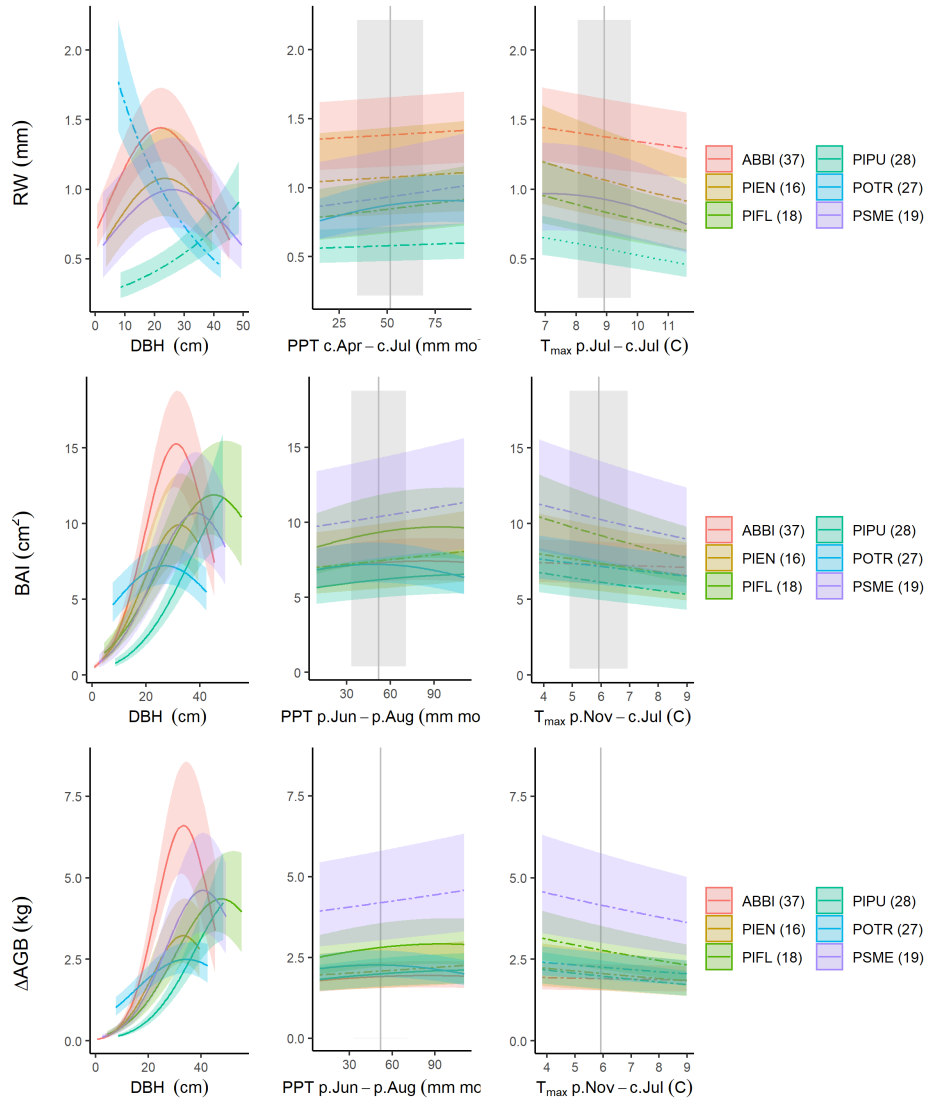


Figure S17. Best GLS models for Cedar Breaks (Utah, USA) for all three growth metrics examined here. Precipitation and temperature group variables are as selected by *climwin* (*p*=previous year, *c*=current year). For each species, relationships are plotted if included in top model, with best-fit polynomials plotted with solid lines when both first- and second-order terms are significant, dashed lines when only one term is significant, and dotted lines when neither is significant. Transparent ribbons indicate 95% confidence intervals. Vertical grey lines indicate the long-term mean for the climate variable, shading indicates 1 SD.

Figure S18. Best GLS models for Scotty Creek (Northwest Territory, Canada)

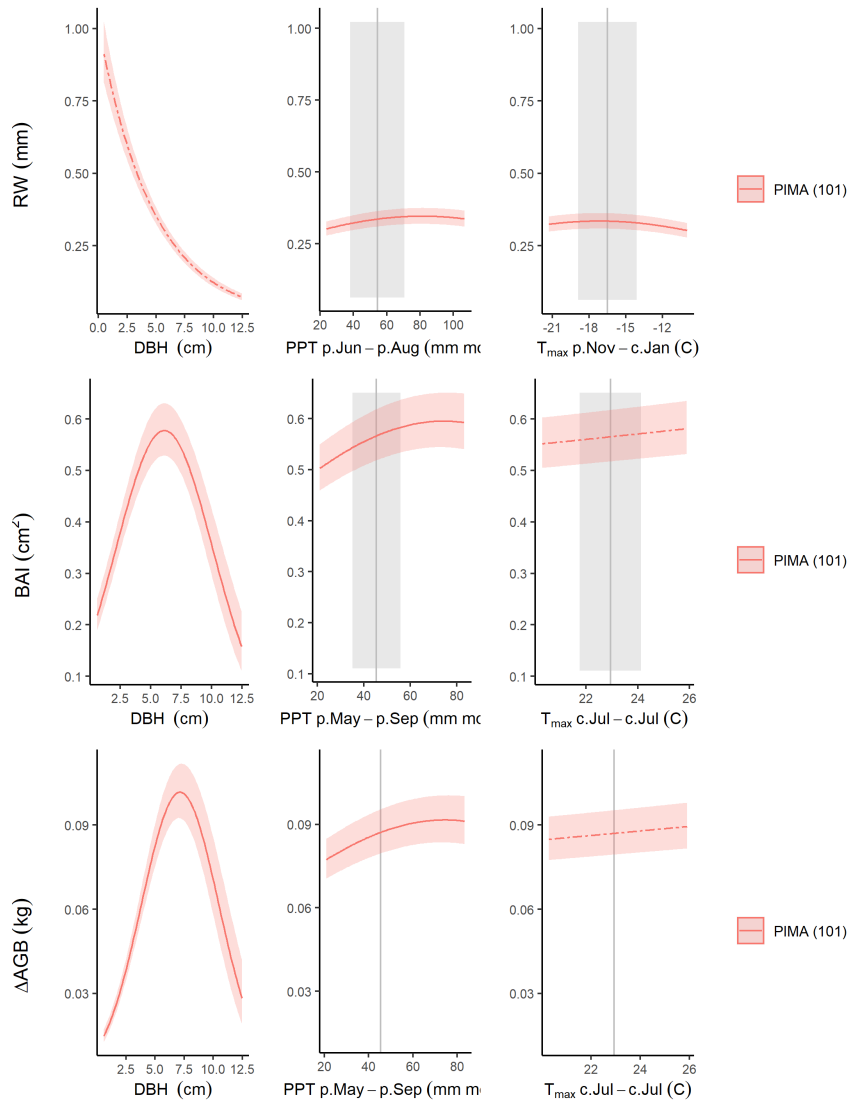


Figure S18. Best GLS models for Scotty Creek (Northwest Territory, Canada) for all three growth metrics examined here. Precipitation and temperature group variables are as selected by *climwin* (*p*=previous year, *c*=current year). For each species, relationships are plotted if included in top model, with best-fit polynomials plotted with solid lines when both first- and second-order terms are significant, dashed lines when only one term is significant, and dotted lines when neither is significant. Transparent ribbons indicate 95% confidence intervals. Vertical grey lines indicate the long-term mean for the climate variable, shading indicates 1 SD.

SI References

- Alfaro-Sánchez, R., Muller-Landau, H. C., Wright, S. J., & Camarero, J. J. (2017). Growth and reproduction respond differently to climate in three Neotropical tree species. *Oecologia*. <https://doi.org/10.1007/s00442-017-3879-3>
- Applequist, M. (1958). A simple pith locator for use with off-center increment cores. *Journal of Forestry*.
- Aus de Ar, R. (2018). Tree Rings of *Pinus ponderosa* and *Juniperus virginiana* Show Different Responses to Stand Density and Water Availability in the Nebraska Grasslands. *The American Midland Naturalist*, 180(1), 18. <https://doi.org/10.1674/0003-0031-180.1.18>
- Bumann, E., Awada, T., Wardlow, B., Hayes, M., Okalebo, J., Helzer, C., Mazis, A., Hiller, J., & Cherubini, P. (2019). Assessing responses of *Betula Papyrifera* to climate variability in a remnant population along the Niobrara River Valley in Nebraska, U.S.A., Through dendroecological and remote-sensing techniques. *Canadian Journal of Forest Research*, 49(5), 423–433. <https://doi.org/10.1139/cjfr-2018-0206>
- Charney, N. D., Babst, F., Poulter, B., Record, S., Trouet, V. M., Frank, D., Enquist, B. J., & Evans, M. E. K. (2016). Observed forest sensitivity to climate implies large changes in 21st century North American forest growth. *Ecology Letters*, 19(9), 1119–1128. <https://doi.org/10.1111/ele.12650>
- Cook, E. R. (1985). *A Time Series Analysis Approach to Tree Ring Standardization: Vol. Ph.D* [PhD thesis]. University of Arizona.
- Cook, E. R., & Kairiukstis, L. A. (Eds.). (1990). *Methods of Dendrochronology: Applications in the Environmental Sciences*. Springer Netherlands. <https://doi.org/10.1007/978-94-015-7879-0>
- Cook, E. R., & Peters, K. (1997). Calculating unbiased tree-ring indices for the study of climatic and environmental change. *The Holocene*, 7(3), 361–370. <https://doi.org/10.1177/095968369700700314>
- Duncan, R. P. (1989). An evaluation of errors in tree age estimates based on increment cores in kahikatea (*Dacrycarpus dacrydioides*). *New Zealand Natural Sciences*, 16, 31–37.
- Helcoski, R., Tepley, A. J., Pederson, N., McGarvey, J. C., Meakem, V., Herrmann, V., Thompson, J. R., & Anderson-Teixeira, K. J. (2019). Growing season moisture drives interannual variation in woody productivity of a temperate deciduous forest. *New Phytologist*, 223(3), 1204–1216. <https://doi.org/10.1111/nph.15906>
- Jones, P. D., Osborn, T. J., & Briffa, K. R. (1997). Estimating sampling errors in large-scale temperature averages. *Journal of Climate*, 10(10), 2548–2568.
- Kašpar, K., Tumajer, J., Vašíčková, I., & Šamonil, P. (n.d.). *Species-specific climate-growth interactions determine the future tree species dynamics of the mixed Central European mountain forests*.
- Maxwell, J. T., Harley, G. L., & Robeson, S. M. (2016). On the declining relationship between tree growth and climate in the Midwest United States: The fading drought signal. *Climatic Change*, 138(1-2), 127–142. <https://doi.org/10.1007/s10584-016-1720-3>
- Niinemets, Ü., & Valladares, F. (2006). Tolerance to shade, drought, and waterlogging of temperate northern hemisphere trees and shrubs. *Ecological Monographs*, 76(4), 521–547. <https://doi.org/10.6084/m9.figshare.e.c.3309258.v1>
- Paton, S. (2019). *Barro Colorado Island, Clearing_Precipitation, manual*. The Smithsonian Institution. <https://doi.org/10.25573/data.10042502.v3>
- Sniderhan, A. E., & Baltzer, J. L. (2016). Growth dynamics of black spruce (*Picea Mariana*) in a rapidly thawing discontinuous permafrost peatland: Growth Dynamics Boreal Peatlands. *Journal of Geophysical Research: Biogeosciences*, 121(12), 2988–3000. <https://doi.org/10.1002/2016JG003528>
- Tumajer, J., Altman, J., Štěpánek, P., Treml, V., Doležal, J., & Cienciala, E. (2017). Increasing moisture limitation of Norway spruce in Central Europe revealed by forward modelling of tree growth in tree-ring network. *Agricultural and Forest Meteorology*, 247, 56–64. <https://doi.org/10.1016/j.agrformet.2017.07.015>

Vlam, M., Baker, P. J., Bunyavejchewin, S., & Zuidema, P. A. (2014). Temperature and rainfall strongly drive temporal growth variation in Asian tropical forest trees. *Oecologia*, 174(4), 1449–1461. <https://doi.org/10.1007/s00442-013-2846-x>

Williams, A. P., Allen, C. D., Macalady, A. K., Griffin, D., Woodhouse, C. A., Meko, D. M., Swetnam, T. W., Rauscher, S. A., Seager, R., Grissino-Mayer, H. D., Dean, J. S., Cook, E. R., Gangodagamage, C., Cai, M., & McDowell, N. G. (2012). Temperature as a potent driver of regional forest drought stress and tree mortality. *Nature Climate Change*. <https://doi.org/10.1038/nclimate1693>